CERN / DRDC 94-47
RD36 - Status Report
January 9th 1995

A Shashlik + Preshower Detector as Electromagnetic Calorimeter For LHC

RD-36 Collaboration

P. Aspell, S. Bates, Ph. Bloch[1], R. Grabit, P. Jarron, F. Lemeilleur, R. Loos, A. Marchioro, E. Rosso
CERN, Geneva, SWITZERLAND

S.R. Chendvankar, S.K. Gupta, S.N. Ganguli, A. Gurtu, M. Maity, G. Majumder, K.Mazumdar, T. Moulik
EHEP Group, Tata Institute of Fundamental Research, Colaba, Bombay, India

R.M. Brown, D.J.A. Cockerill, J. Connolly, L. Denton, R. Stephenson
Rutherford Appleton Laboratory, Didcot,UK

I. Cheremukhin, A. Egorov*, I. Golutvin, Y. Kozlov*, P. Moissenz, S. Sergueev, A. Sidorov*, E. Zubarev, N. Zamiatin
JINR, Dubna, RUSSIA

K. Kloukinas, N. Siolios, F. Triantis
University of Ioannina, Ioannina , GREECE

P. Bordalo, S. Popov, S. Ramos, J. Varela
LIP, Lisboa, PORTUGAL

L. Alcacer, J. E. Franca, C. Azeredo Leme, J. Cordeiro Vital
IST Centre , Lisboa, PORTUGAL

E. Clayton, D. Miller, C. Seez, T.S. Virdee
Imperial College, London, UK

R. Djilkibaev, S. Gninenko, E. Guschin, Y. Musienko, V. Popov, A. Skasyrskaya, I. Semenyuk
INR, Moscow RUSSIA

S. Abdullin, V. Kaftanov, V. Lukashin, A. Nikitenko, Y. Semenov, A. Starodumov, N. Stepanov, Y. Trebukhovsky
ITEP, Moscow RUSSIA

J. Badier, A. Busata, Ph. Busson, C. Charlot, L. Dobrzynski[2], O. Ferreira, Ch. Gregory, A. Karar, P. Manigot, R. Tanaka, J.Ch. Vanel
Ecole Polytechnique, Palaiseau, FRANCE

S. Bityukov, V. Obraztsov, A. Ostankov, Yu. Protopopov, V. Rykalin, P. Spiridonov, V. Soushkov, V. Vasil'chenko
IHEP, Moscow RUSSIA

B. Brower, A. Dominguez, Ch. Duba, H. Paar
University of California, San Diego,USA

N. Godinovic, I. Puljak, I. Soric
FESB, University of Split, Split , Croatia

O. Dubois, O. Ganel, R. Wigmans
Texas Tech University, Texas, USA

P. R. Hobson, D. C. Imrie
Brunel University, Uxbridge, UK

---

[1] Contact person
* Elma Industry, RUSSIA
[2] Spokesperson

Abstract

The aim of the RD36 collaboration is to develop a lead scintillator sampling calorimeter read by wave length shifting fibres (Shashlik calorimeter) and its associated Silicon strip preshower, and to study their possible implementation in the CMS detector.

In 1994, the collaboration has performed measurements of the energy and position resolutions of various prototypes within or without magnetic field. The measured resolution is defined by a stochastic term of $8.5\%/\sqrt{E}$ (E in GeV), a noise term of $.330/E$ and a constant term of 0.5%. The shower angular resolution is better than 70 $\text{mrad}/\sqrt{E}$.
The reproducibility of the tower performances and the uniformity of the calorimeter response have been studied on a large (25x25 cm^2 cross section) newly built prototype.
New preamplifiers and chips for the Silicon strips readout have been produced and tested.
A mechanical design for the CMS Barrel and End-Caps ECAL has been prepared.

Table of Contents

1. Introduction

The benchmark for an electromagnetic calorimeter at LHC is the detection, at high luminosity, of an intermediate mass Higgs boson through its two photon decay.

In the Standard Model there is an important mass range ($90 < m_H < 130$ GeV) in which only this channel can be seen. In the Minimal Super Symmetric extensions to the Standard Model this channel allows also an exploration of a large fraction of the parameter space inaccessible to LEP II ($\sqrt{s} = 190$ GeV). To detect the Higgs two photon decay, the electromagnetic calorimeter needs excellent energy resolution and a good rapidity coverage. An efficient rejection of neutral pions and the measurement of the angle of incidence of the photon in the r-z plane ("photon pointing") are also required[1.1].

Using the design parameters of the CMS Shashlik electromagnetic calorimeter:

- Stochastic term = $9\%/\sqrt{E}$ (GeV),
- Constant term = 1%,
- Noise = $300/E$ (MeV),
- Angular resolution = $70\text{mrad}/\sqrt{E}$ (GeV)

a signal from a Standard Model Higgs for $m_H > 85$ GeV, with a statistical significance of more than 5σ, can be observed. Figure 1 shows (result of a single Monte-Carlo experiment for 10^5 pb^{-1}) how SM Higgs of masses 90, 110, 130 and 150 GeV would look after background subtraction. For more details of this analysis see reference [1.2] and references therein.

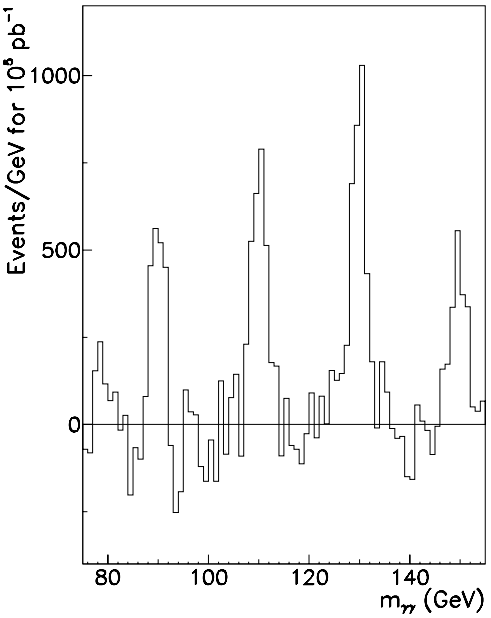

Figure 1: *Result of a single Monte-Carlo experiment for 10^5 pb^{-1} with Higgs peaks at 90, 110, 130 and 150 GeV.*

The main goals of RD36 [1.3] work were:

- to prove that the design performance could be achieved for a large scale prototype and so extrapolated to a full size LHC detector,
- to demonstrate that the tower construction technique could provide a high quality detector at a low cost,
- to produce prototypes of the readout electronic for the silicon preshower, necessary for the photons direction reconstruction and π^0 rejection,
- to develop a performent hermetic mechanical design for the electromagnetic calorimeter and the preshower,
- to study the radiation tolerance of the tower components.

In the present report, we will first describe the different prototypes (calorimeter and preshower) used for test beam studies. The achieved results obtained without magnetic field and in a high magnetic field (3 Tesla) will be reported in section 2. It will be shown that the minimal design parameters have been easily achieved in all experimental conditions. Section 3 gives the status report of the work performed on the preshower readout electronics. In section 4 are shown the mechanical designs for the Barrel and the End-Caps calorimeters fulfilling the CMS detector constraints (limited radial space in a 4 Tesla magnetic field), as well as the main lines of the preshower design.

The proposed calorimeter has to satisfy the LHC physic's requirements. Essential conditions are the technical feasibility and the robustness of the calorimeter mechanics and its electronics components. The final cost of the detector is also an important element in the choice. Optimisation of the relevant parameters can be carried out by referring to the measurement quality of the gamma's in the 50-200 GeV range. Three quantities may characterise the performance of the detector. The first one is the precision on the energy measurement (dE/E), the second one is the precision on the position determination and the last one is the proportion of photons lost due to fiducial geometric acceptance. These three topics will be discussed in this report using the achieved performances for the Shashlik calorimeter as well as Monte Carlo simulations [1.4].

2. Main characteristics of a Shashlik calorimeter

2.1. RD36 prototypes

The Shashlik calorimeter is based on a technique to readout the scintillation light of a lead/scintillator plate sampling calorimeter with the use of WLS fibres running perpendicular to the plates through holes in the plates. Different kinds of towers were built and studied during the last 2 years. Their parameters are summarised in Table 1. They differ in size, WLS fibre type and assembly technique: stainless steel rods running through additional holes, four stainless steel straps {50 and/or 100μm thick} welded on a stainless steel front and back plate or aluminium foils (50-125 μm thick) glued on the lead tiles and on a front and rear holding piece). The towers were wrapped either with aluminium or aluminised mylar. To separate lead from scintillator either ordinary white paper or Tyvek was used.

	NONET (parallelipedical)	**OLD-PROJECTIVE** (projective η=0)	**NEW IHEP** (projective η=0)	**Glued towers** (at large η)
Number of towers	9	16	36	6 (EP) + 7 (INR)
Tower lateral size	47 x 47 mm^2	52 x 52 mm^2	42 x 42 mm^2	trapezoidal size
Number of planes	75		70	80
Total depth	27.5 X_0		25.7 X_0	29.3 X_0
Radiation length	16.9 mm		16.2 mm	
Moliere radius	34 mm			
Lead thickness	2 ± .005 mm		2 ± .002 mm	
Scintillator type	Polystyrene + .5% POPOP		+2%Para-Terphenyl	
Scint. thickness	4 ±.05 mm		3.74 ±.01 mm	
WLS fibres	Y7	K27 and Y7	Y11	Y7
Number of fibres	25	36		
Fibre pitch	9.5 mm		7 mm	
Fibre diameter	1.2 ±.03 mm		1.0 ±.03 mm	.83 ±.03 mm
Hole Φ in scint.	1.3 mm		1.2 mm	1.0 and 1.2 mm
Hole Φ in lead	1.5 mm		1.2 mm	1.0 and 1.2 mm
Front fibre Ends	Aluminised	Loops	Aluminised	
Light yield	12 γ / MeV		20 γ / MeV	not measured

Table 1: *Main parameters of CMS prototype Shashlik towers.*

Shashlik calorimeter prototypes equipped with pre-shower detector have been tested in electron, muon and pion beams at CERN-SPS. In the design of the CMS detector at LHC, the electromagnetic calorimeter operates inside a strong magnetic field (4 Tesla). It is therefore very important to test the whole Shashlik and preshower system in a magnetic field. We have tested the projective towers (OLD-PROJECTIVE) in a 3 Tesla field generated by EHS magnet at SPS-H2 beam line during April-May 1994. During the Spring of 1994, new projective Shashlik modules (NEW IHEP) were constructed with special attention to mechanical tolerances.

These new towers had smaller lateral dimensions than the older ones and the fibre density was also changed. These new towers have been tested at SPS-H4 beam line with a preshower detector during July-September 1994.

All these towers were equipped with a 10x10mm^2 silicon PIN photodiode readout (S3590 Hamamatsu) followed by a low noise amplifier designed at INR. Typically we have taken data with a shaping of 30-40 ns and a gate width of 160-200ns.

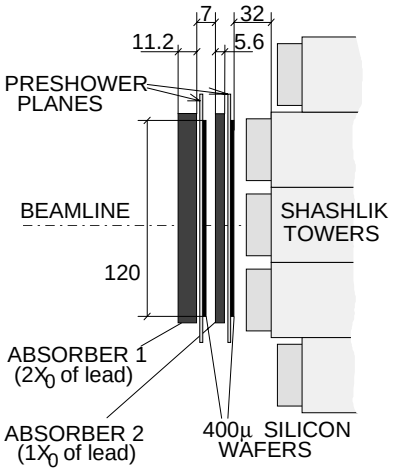

Figure 2: *Test beam setup. Shashlik towers with preshower*

in front (dimensions in mm).

The light yield of first set of prototype towers was 12 γ/ MeV. For the NEW IHEP ones, a light yield of 20 γ/ MeV was achieved . This increase comes from several factors: better quality of the construction, use of multiclad fibres and special tyvek for lead / scintillator separation.

Figure 2 shows the standard setup in the beam: a matrix of calorimeter towers with, in front, a preshower detector containing 2 planes of silicon strip detectors. Each preshower plane was built out of 4 wafers (6 x 6 cm^2 each) with $2X_0$ ($1X_0$) absorber in front. The preshower was readout by a 16-channel Amplex-SICAL signal processor [2.1]. Each wafer was connected to a printed board circuit containing two AMPLEX's. The analog signals from the strip wafers are used to find the position of the shower and to correct for the energy lost in the absorber material.

We will first report the results obtained with a 3x4 tower matrix (OLD-PROJECTIVE) placed in the EHS magnet [2.2] for the studies of magnetic field effect on the calorimeter+preshower response ,and then study a matrix of 6 x 6 projective towers (NEW IHEP) (figure 3) placed in the H4 beam line. The central towers Tower 15, 16, 21 and 22 were exposed to electrons with various energies to study the energy resolution. Tower-21 is a special since the WLS fibres are also projective (thus fibre density varies as a function of the depth of the shower inside the tower). In all other towers the distance between fibres (parallel WLS fibres) is constant, permitting some compensation between light collection efficiency (less efficient for later shower development) and light loss due to attenuation in fibre. For uniformity study, the full surface of 6x6 matrix was scanned with a 80 GeV electron beam (see references [2.3 - 2.10])

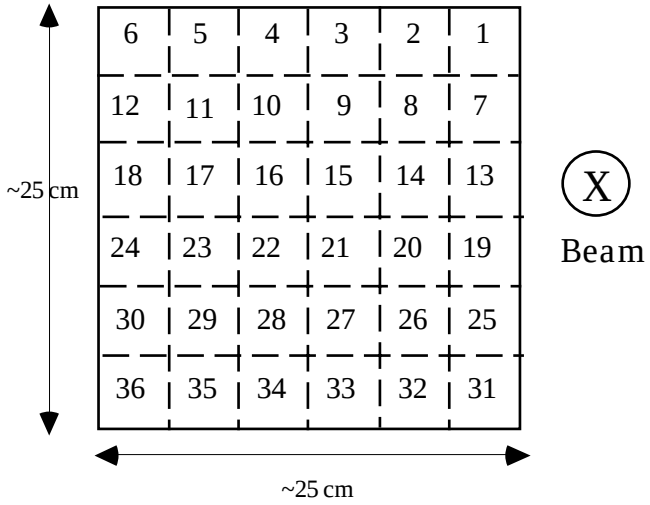

Figure 3: *6 x 6 Shashlik tower matrix tested in in H4-SPS beam line. The towers front dimensions are 42x42 mm^2 giving at the shower maximum an apparent size of 48x48 mm^2*

Some data with pions (50 GeV) and muons (225 GeV) were also taken to study response to mip and hadronic showers.

2.1.1. Quality of the towers

To evaluate the quality of the towers, we have measured their response to a Cobalt 60 radioactive source. Data were taken every 2 cm from the front to the rear of the tower. The towers were read out with a PMT connected to a multimeter. Figure 4 gives the mean light response when the response was averaged between z=6 and 36 cm (see figure 5). The dispersion for all the towers (taking out tower 33 and 36 for which we have used .83 mm diameter Y7 fibres) is ±7%. When the longitudinal profile measurements of each tower were normalised to the mean light response shown on figure 4, one obtains the results presented in figure 5. The small dispersion in these measurements indicates the good quality of the towers.

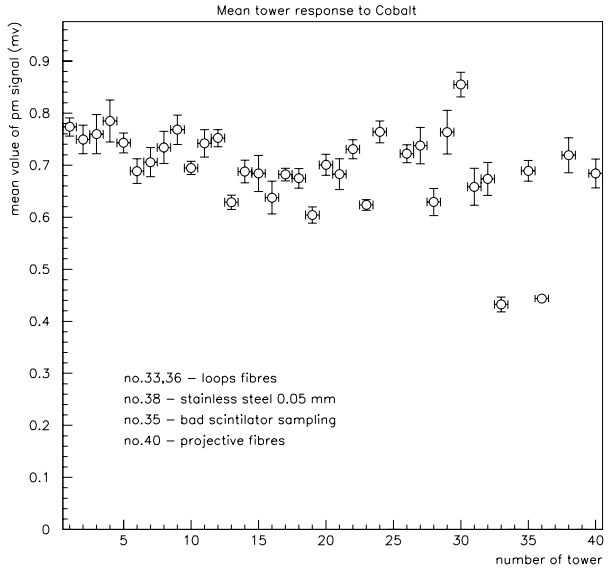

Figure 4: *Mean light response for the 36 NEW IHEP towers.*

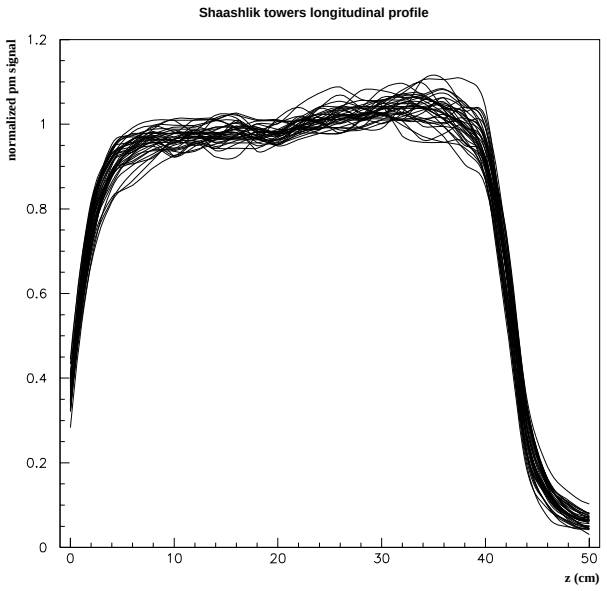

Figure 5: *Longitudinal light response for the 36 NEW IHEP towers.*

2.2. Calorimeter Readout Electronics.

Figure 6 shows the diagram of the readout electronics used in the test beam. The PIN detector characteristics are given in table 2. The preamplifier will be described in more detail below. The differential amplifier G1, with adjustable gain, compensates losses in the transmission line and allows to adjust the global gain on each channel. The amplifier G1 is followed by the amplifiers AL and AH with gain 1 and 10 respectively. Low level and high level signals are measured with the 12(11) bits converters ADC 1 and ADC 2 respectively (FERA at H4 beam line).

Active area	9*9 mm2
Thickness	500m
Capacitance at full depletion bias	27 pF
Full depletion bias	80 V
Leakage current	< 8 nA
Quantum efficiency	68% (at = 550 nm)

Table 2: *Main characteristics of HAMAMATSU (S3590-05) photodiode*

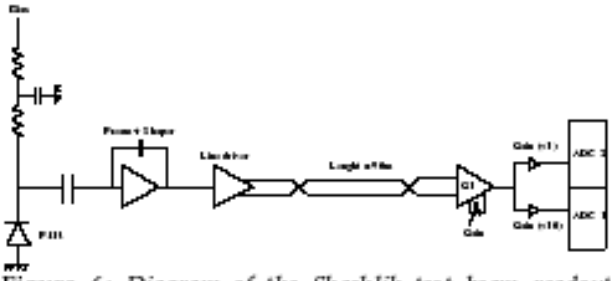

Figure 6: *Diagram of the Shashlik test beam readout electronic.*

2.2.1. *Preamplifier-Shaper-Line Driver*

In the PIN photodiode the electron-hole pairs directly produced by the scintillation light constitute the charge signal (typically 10-13 electron-hole pairs created per MeV of energy loss in the Shashlik calorimeter). So the use of low-noise amplifier is required.

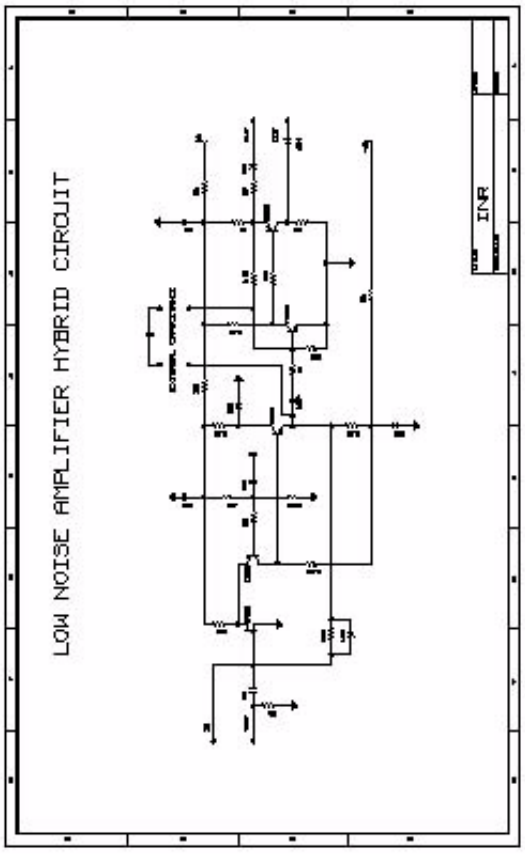

Figure 7: *Diagram of the low noise charge amplifier hybrid circuit.*

Also fast shaping of signals is required to keep the noise from energy pile-up small. The equivalent noise charge of the amplifier depends directly on the noise performance of the first transistor and on the detector's characteristics. A JFET KP341, characterised by high transconductance (25 mA/V) and low input capacitance (5 pF) has been chosen because of its best low-noise performances for the detector capacitance in the range 0-50 pF. A fast low-noise charge amplifier has been designed as a hybrid variant. The overall linear chain of the amplifier is shown in Figure 7. The second stage provides additional amplification and cancellation of the signal tail that reduces the signal length to 30 ns.

Figure 8 presents a typical delta current response of the amplifier for 2 different capacitance's of detector. The design allows to increase the shaping time of the amplifier using an external capacitance.
The ENC of the hybrid amplifier was measured for several detector capacitance's, up to 70 pF. The results are shown in Figure 9. The measured overall gain of the amplifier is 5.4 mV/fC. For the 9*9 mm2 (C_d = 27 pF) active area Hamamatsu photodiode (S3590-05) we measured 1300 electrons equivalent noise charge.

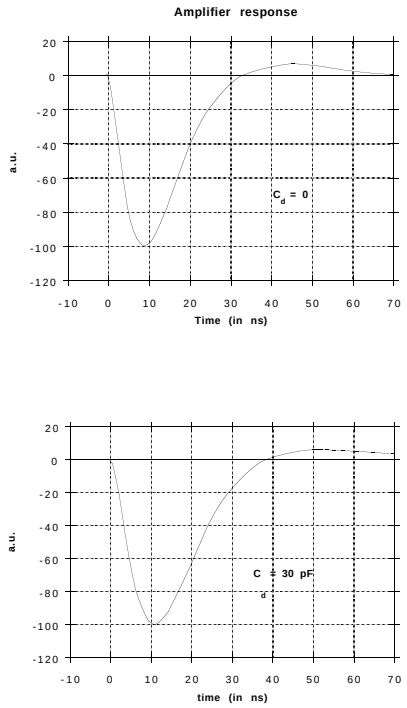

Figure 8 : *Current response of the hybrid amplifier for 2 different detector capacitance (0 and 30 pF).*

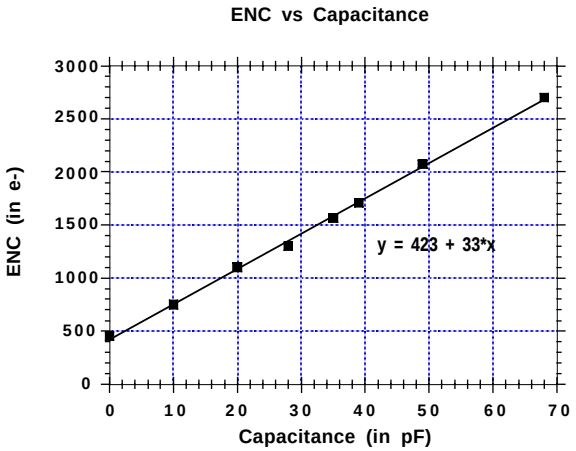

Figure 9: *ENC of the hybrid amplifier as function of the detector capacitance.*

The maximum negative output voltage swing of this amplifier is 2.5V. Its power consumption, determined essentially by the second stage is about 400 mW per channel.
The linearity performance for a gate width of 50 ns, is better than ±1% in the range 10^3-2 10^6 electrons at the input. Almost all Shashlik tests were done using this amplifier.

Another surface mounted hybrid was designed and tested. There are two versions of this amplifier. One with a radiation- resistant JFET-NJ450 and another with a bipolar transistor KT640 at the input.

This amplifier has a high dynamic range (up to 8V negative voltage swing) and provides excellent linearity. Simulated and measured linearity are better than ±0.5% for a dynamic range from 10^3-10^7 electrons. The dependence of the noise versus the detector capacitance is shown in Figure 10. The amplifier has fast response (25 ns at the baseline) and high gain (6mV/pC). This amplifier was also used for some Shashlik calorimeter tests.
The circuit version with bipolar transistor is given in reference [2.10].

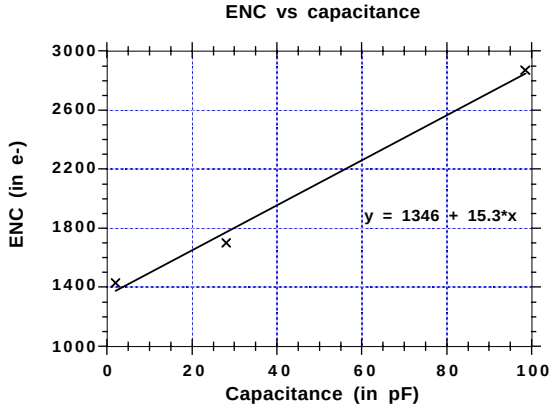

Figure 10: *ENC of the large dynamic range amplifier used for some Shashlik measurements. This amplifier is described in reference [2.10]*

2.3. Study of the Shashlik response uniformity

2.3.1. Data

An intensive study of the bare Shashlik uniformity was performed on the 6 x 6 matrix (NEW IHEP) with 80 GeV electron beam initially without preshower. An area of 20 x 15 cm^2 was illuminated with a density of about 150 events / mm^2. The objective was to study the energy measurement response ($\Sigma_{9\ towers}$) all over the tower area and in particular around fibres and at the edges of the towers. Figure 11 shows the tower limits and the area which was exposed to the electron beam and used for the energy measurements. Eight towers have been completely covered and eight others from the tower edge up to the centre. Data were also taken in the towers located at the edge of the matrix but they could not be used for energy reconstruction due to lateral energy leakage.

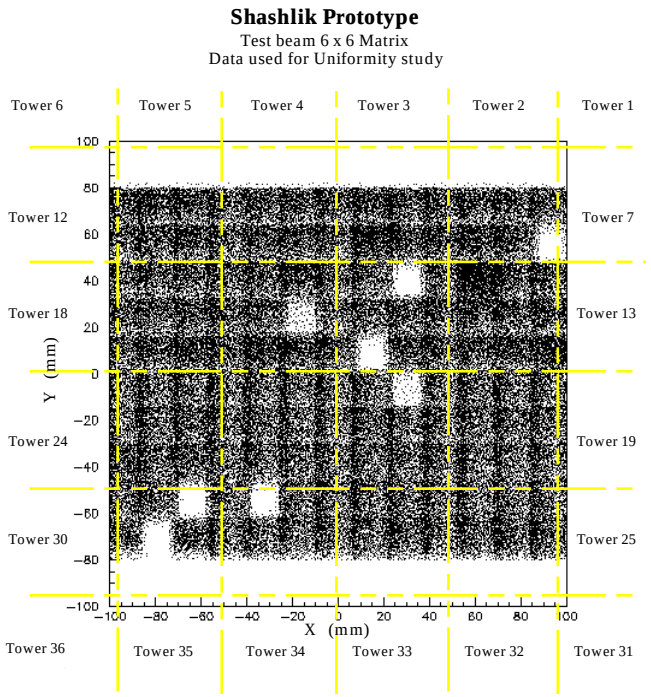

Figure 11: *Sketch of the 6x6 test beam Shashlik matrix and the 80 GeV electron data (5 10^6 triggers) taken for the uniformity study. The empty squares correspond to unusable data files.*

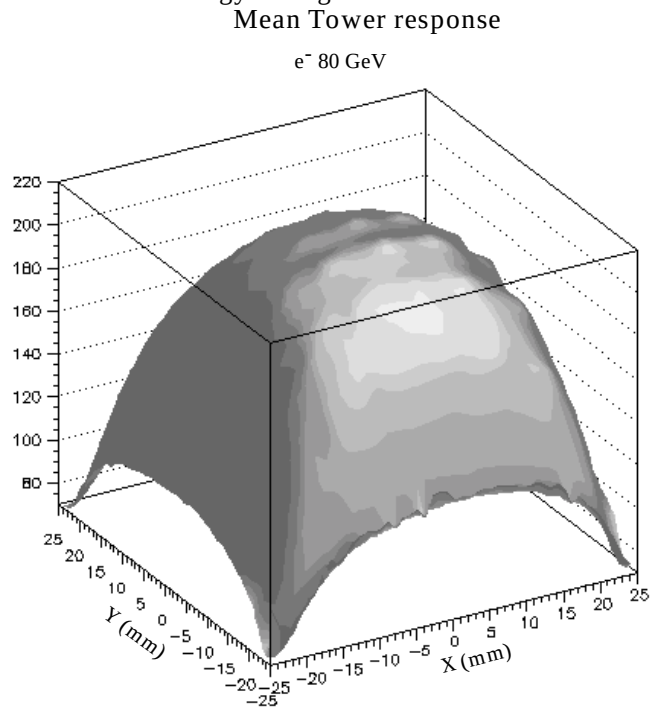

Figure 12: *Mean response of single towers obtained by averaging the response of 24 towers exposed to 80 GeV electrons.*

2.3.2. Single tower response

A first study on all individual towers was performed with 80 GeV electrons .

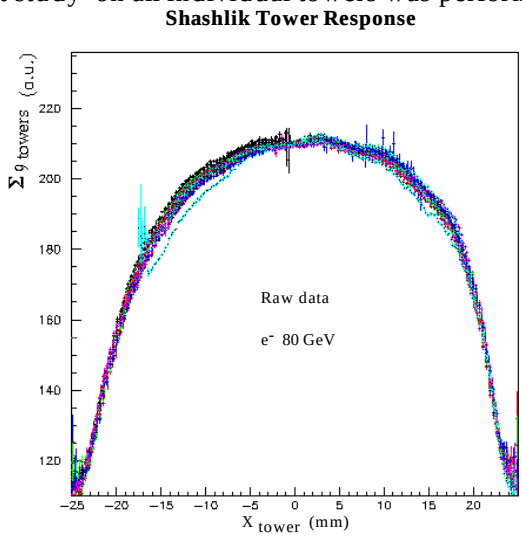

Figure 13: *Superimposed response of 24 Shashlik towers exposed to 80 GeV electrons. The slices are running through the tower centre including data with Y = ± 10mm. Similar results were obtained for X slices in the Y projections.*

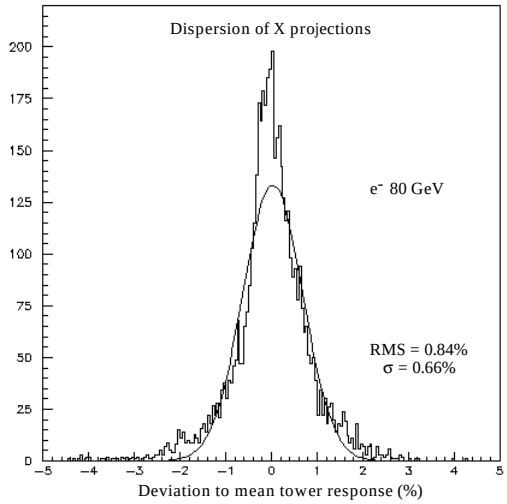

Figure 14: *24 Shashlik towers exposed to 80 GeV electrons: deviation of the data shown on figure 13 to its mean value. For the y projection we obtained an RMS= 0.72% (σ =0.53%)*

Figure 12 shows the mean response for 24 towers. One can notice the remarkable symmetry of the response due to the good tower quality. Figure 13 gives the x slice of this response for a range of y = ±10 mm going through the tower centre. Data for 24 towers have been superimposed. The small undulations apparent in the data are expected from the WLS fibres. The distance between fibres is 7 mm.
The lateral scan indicates a tower size of 47.7 mm which is some what larger than the physical size (42 mm). This is due to the projective shape of the towers and the size we observe is the one near the shower maximum. The tower to tower dispersion is small. It can be evaluated from figure 14, where we have plotted the deviations (in percent) of each point of figure 13 (250 per tower) to the mean value at this point. All the data have a mean dispersion of ±0.84% (±0.72% for the Y slice[2.10]). The small difference between X and Y dispersions can be explained by the fact that our setup is tilted by 3 degree in X (angle between the incident electron and the fibre axis) and is fully projective in y inducing a more important fibre channelling. From this study we also tried to estimate the dead space between towers. From the X profiles, we found some loss in energy measurement over 0.2 mm. For Y, the losses were larger (no tilt) and spread over 0.5-1.0 mm. This will be discussed in more details in section 2.3.5.

2.3.3. Uniformity of the calorimeter response

The non uniformity is studied using the shower reconstructed energy which is the sum of the deposited energy in 9 towers.
Figure 15 gives the averaged response of the 16 towers for which deposited energy can be reconstructed. Figure 16 shows the superposition of the response for 16 individual towers when X slices for a range of Y = ±10 mm are studied.
Part of the dispersion is due to differences in calibration when the sum of 9 towers is considered, but it is clear that a 2^{d} order polynomial shape can be used to adjust the responses.

A deviations of 0.71% (0.72%) from the mean value, at each point, for x (y) is obtained (figure 17), confirming the deviations from tower to tower described above.

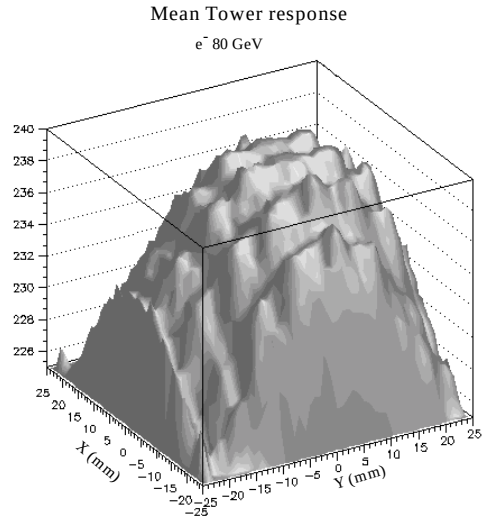

Figure 15: *Mean response (Σ of 9 towers) for the 16 central towers of the 6x6 matrix exposed to 80 GeV electrons. The dispersion of all the data is ±3%.*

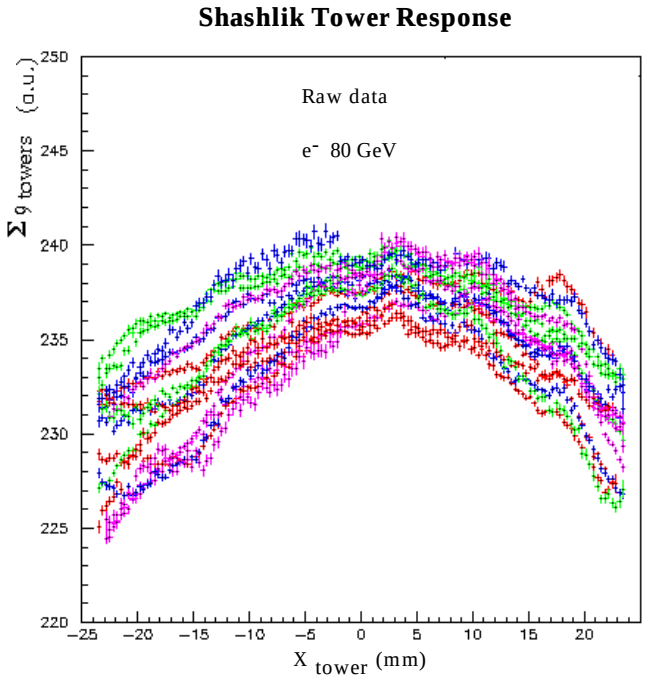

Figure 16: *Superimposed response of 16 Shashlik towers exposed to 80 GeV electrons. Data for the full tower are used (ΔY= 47 mm). Similar distribution was obtained for the Y projection.*

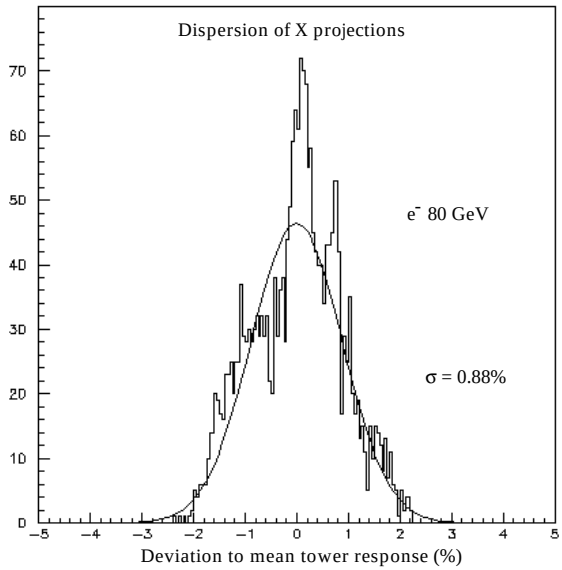

Figure 17:*16 Shashlik towers exposed to 80 GeV electrons: deviation of the data shown on figure to their mean response. For the Y projection we got a* σ*=0.67%.*

2.3.4. *Uniformity correction*

Knowledge of the lateral uniformity of response is a crucial issue for the energy resolution and the calibration of a calorimeter involving more than ten thousands towers. The lateral non uniformity is mainly caused by the variation in the quality of the tower construction, non-uniform reflectivity at the side of the tiles and due the choice of parallel fibres implying that the distance between the fibres and scintillator edges changes from the front to the rear of the tower. This last effect can be compensated by an appropriate choice of the fibre attenuation length. There also exists a local non uniformity around the fibres. But this problem can be avoided by tilting the tower by a few degrees with respect to the incident beam angle.
We have parametrized the x (y) slices of the tower responses by a second order polynomial modulated by a sine wave:

$$f(E) = a_1\langle 1 - a_2(x - a_6) - a_3(x - a_6)^2\rangle\langle 1 - a_4\cos(\frac{(2\pi(x - a_6)}{a_5})\rangle$$

where a_1 is the tower response at its centre, $a_2(a_3)$ the global non uniformity correction, a_4 the amplitude of the undulation due to the fibres, a_5 the distance between the fibres and a_6 the tower centre position. The quadratic term represents the main correction to be applied to the data. The response after corrections for the same 16 towers are shown in figure 18 and 19 for the x and y projections respectively. The overall dispersion is now small (≈0.3%). Detailed discussions of uniformity corrections are given in reference [2.10].

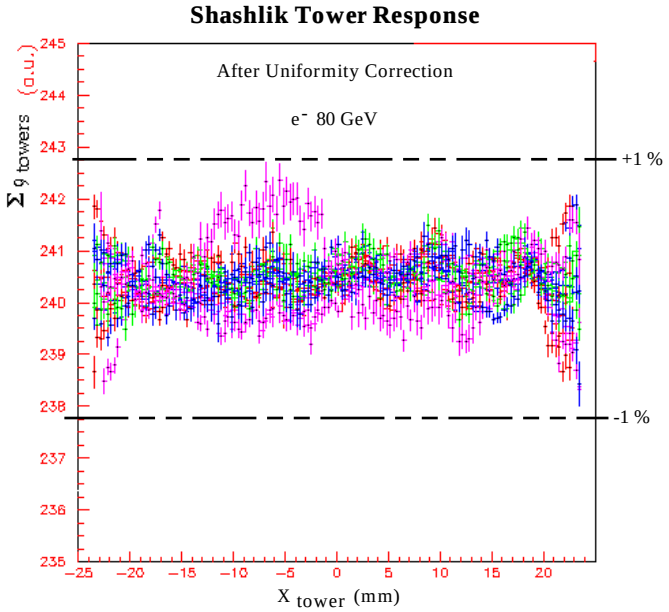

Figure 18: *Superimposed response of 16 Shashlik towers exposed to 80 GeV electrons. Data for the full tower are used (ΔY= 47 mm). The dispersion of all the data to the mean response has a σ = 0.14%.*

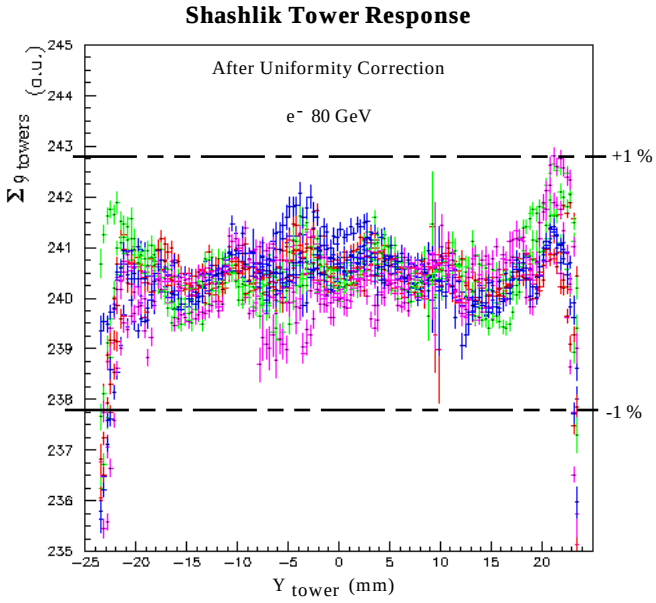

Figure 19: *Superimposed response of 16 Shashlik towers exposed to 80 GeV electrons. Data for the full tower are used (ΔX= 47 mm). The dispersion of all the data to the mean response has a σ = 0.16%.*

One sees that for the X projection (3 degree tilt) all the effect of the fibres is absorbed. For the Y projection our correction of the fibre effect is not completely efficient, an undulation is still observable but its amplitude is small. One can also remark on figure 19 (Y slice) that the edges effect due to non tilted cracks is more pronounced than for the tilted direction (X slice).
A similar study was performed with 150 GeV electron data. With the same corrections the dispersions for the X(Y) projections are characterised by a σ = 0.18%(0.17%) respectively. Detailed results are reported in reference [2.10].

2.3.5. *Tower to tower cracks.*

The large amount of data allows the study, on several groups of towers, the influence of tower to tower cracks on the energy resolution. As already seen the 3 degree tilt is large enough to cancel the effect due to inactive materials (stainless steel straps, mylar, air ...) present between 2 adjacent towers. The losses due to projective cracks are larger in the non tilted direction as it can be seen on figures 19 and 20. The effect is at maximum 3%. The overall region over which the effect extends is about ±1 mm. However with the 3 X_0 preshower absorber in front the effect of the cracks is reduced by a large factor as can be seen on figure 21. Its total magnitude is now below 1% over a region of less than 0.5 mm.
The effect of these cracks on the H--> γ γ inefficiency is discussed in reference [1.4].

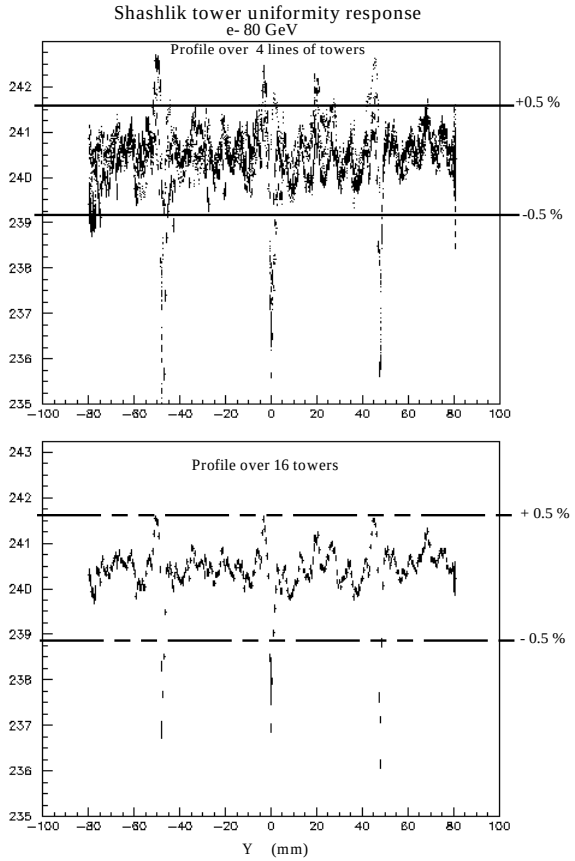

Figure 20: *Uniformity profiles for vertical lines (non tilted) running through 4 towers each. Upper plot: data from 4 line scans superimposed. Lower plot: all data averaged*

2.3.6. Data with preshower

As expected the uniformity of the response for the Shashlik data is improved when a 3 X_0 preshower is present in front of the calorimeter. Figure 22 shows the results obtained for the 6 towers after use of the corrections obtained for the bare Shashlik towers (15 to 17 and 21 to 23) which were scanned with the preshower. The effect of the fibres is not visible anymore. The total amplitude of the non uniformity is reduced to less than 0.5%. It has to be noted that most of the data used for this particular study have been taken in cracks regions to carefully study the effect of the cracks when the preshower is present in front of the calorimeter. The results are particularly encouraging.

It can be concluded from our present study that, for a Shashlik tower calorimeter tilted by 3 degree in one direction and having in front of it a 3 X_0 preshower, the uniformity of the response is very good, being smaller than $\pm$ 0.5%.

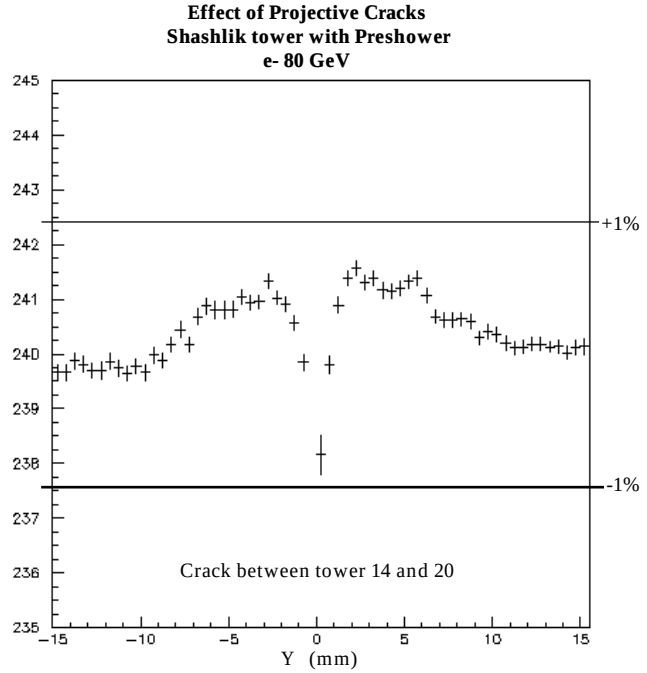

Figure 21: *Crack between tower 14 and 20 (non tilted direction) with the preshower in front*

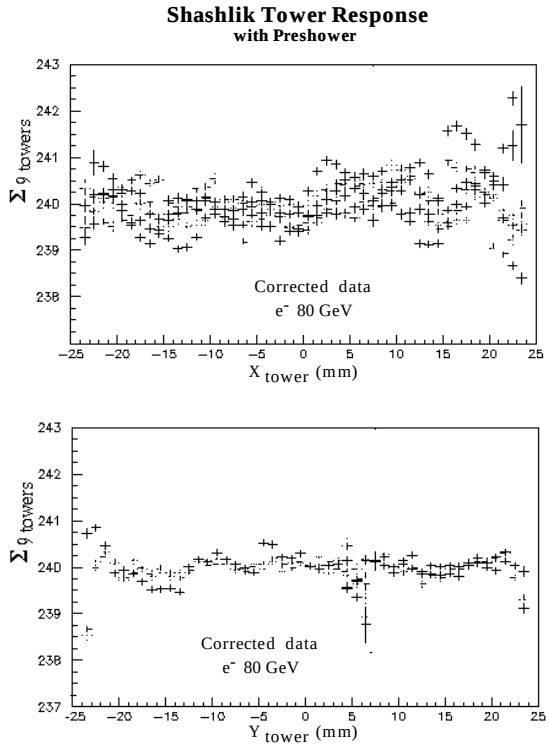

Figure 22: *Superimposed response of 12 Shashlik towers exposed to 80 GeV electrons. Data for the full tower are used (ΔY= 47 mm, and/or ΔY= 47 mm)*

2.4. Shashlik and Preshower in Magnetic Field

As the Shashlik calorimeter is intended to operate in the strong CMS magnetic field, it is of prime importance to study possible consequences on the electromagnetic shower energy measurement. In this section, we analyse the influence of the strong EHS magnetic field on the calorimeter response. The signal distribution, the energy resolution together with longitudinal and transverse profiles are studied. We use data with B=0,1,2,3 Tesla for 150 GeV and 80 GeV electrons with and without preshower in front of the Shashlik (OLD-PROJECTIVE). The quoted field intensity correspond to the maximum field intensity of the EHS magnet. Detailed results are reported in reference [2.9].

2.4.1. Shashlik response in magnetic field

The Shashlik response in magnetic field for Shashlik alone and with 3 X_0 passive material in front is shown in figure 23.
The signals are summed over 9 towers and are normalised to those at 0 Tesla. The light increase can be parametrized as:

$$S = S_0(1+\alpha\sqrt{E})$$

For the 4T CMS field a signal increase of about 13% compared to 0 Tesla should be observed. Such an increase will have to be taken into account for the calibration of the Shashlik modules.
When there is 3 X_0 of passive material in front of calorimeter, the slope is slightly smaller. We have tested that the signal increase is not due to gain variation of the pre-amplifier. One may expect a modification of the electron sampling fraction due to the bending of low energy electrons in the field. A Monte Carlo simulation of the full sampling structure has been performed down to 10 keV electrons and gamma's cut-off. The result is presented in Fig. 24 where signal distributions for 1 GeV electrons without and with a 4 Tesla transverse field are superimposed. No significant difference between 0 and 4 Tesla field is observed. We conclude therefore that the effect is due to an increase of the light yield. Such an effect has already been reported [2.11] for SCSN-38 Kuraray type scintillator, although at lower field intensity (1.5 Tesla). A detailed study on the subject [2.12] already concluded that the phenomena is due to the effect of the magnetic field on base molecule excitation or transfer to the first fluor in the scintillator.

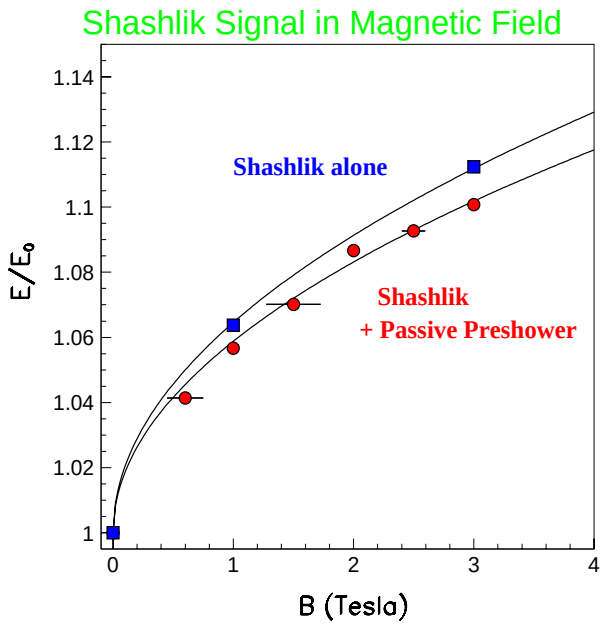

Figure 23: *Shashlik response in the magnetic field for Shashlik alone and with passive preshower 3 X_0 material in front of Shashlik. The curves are to guide the eye.*

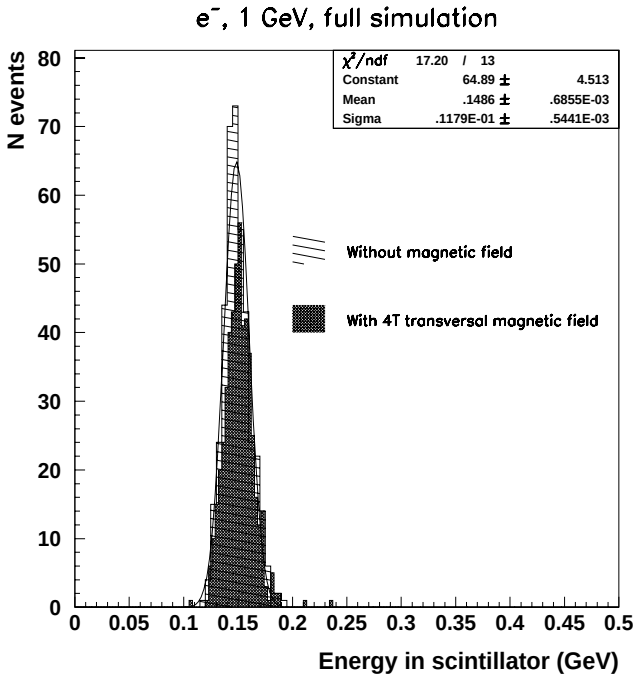

Figure 24: *Energy distribution for 1 GeV electron without magnetic field (dashed and fitted histogram) and with a 4T transversal field, as predicted from Monte Carlo simulation.*

It is shown in reference [2.9] that the relative resolution is not affected by the field.

2.4.2. *Influence on Nuclear Counting Effect*

We observe for high energy showers an excess of events over and above that expected from a gaussian distribution, for values higher than the peak one.. This high energy tail is due to *"leaking"* particles at the rear of the Shashlik modules ($27X_0$ long) that give a signal when traversing the photodiode (see also ref. [2.10]). This tail has been studied as a function of the calorimeter depth and of field intensity. The excess of events is defined as the fraction of events that gives a signal greater than 2 σ above the peak value. The results are plotted in figure 25. We observe that the tail is reduced as expected when increasing the calorimeter depth, but also by a factor three when going from 0 to 3 Tesla magnetic field. This can be understood by the curling of the low energy leaking electrons, at the Shashlik rear due to the field.

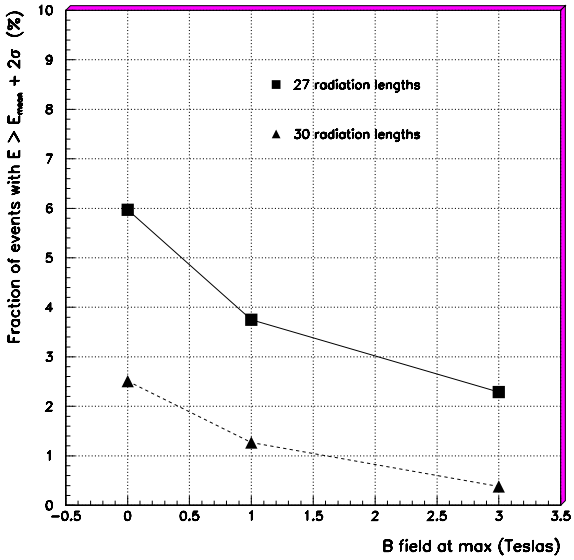

Figure 25: *Excess of high signal events as a function of calorimeter depth and of the magnetic field intensity.*

2.4.3. *Effect on transverse profile*

The shower transverse profile and the calorimeter position resolution without magnetic field has already been reported elsewhere [2.10]. In the magnetic field, one may expect a deformation of the shower profile and therefore a modification of the position resolution. Figure 26 presents the transverse profile for 80 GeV electrons in the direction parallel to the field. The energy in each tower is normalised to the sum and expressed in %, in order to unfold the effect of light increase. Monte Carlo predictions are in good agreement with data. The transverse profile in the direction perpendicular to the field is presented in figure 27 for B=0 and 3 Tesla. One can notice that the initial pattern is asymmetric due to beam incident impact point at -8 mm with respect to tower center. An increase of the lateral spread of the shower in the field is observed in the data, and well reproduced by Monte Carlo. It appears to be symmetrical and amounts to +40 % energy in next to central towers. This implies that the dominating effect of the field on the shower is on electrons / positrons pairs, that is in the high energy part of the shower.

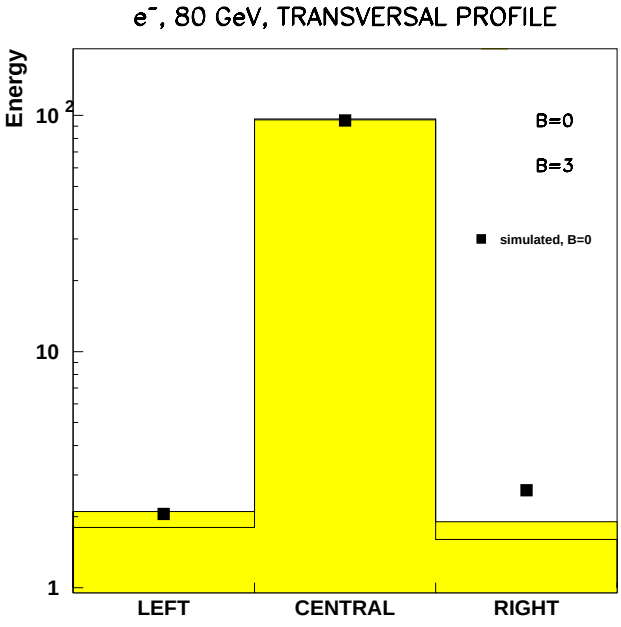

Figure 26: *Transverse profile in the direction parallel to the field for 80 GeV electrons and compared with Monte Carlo simulation without field. Energy is normalised in %.*

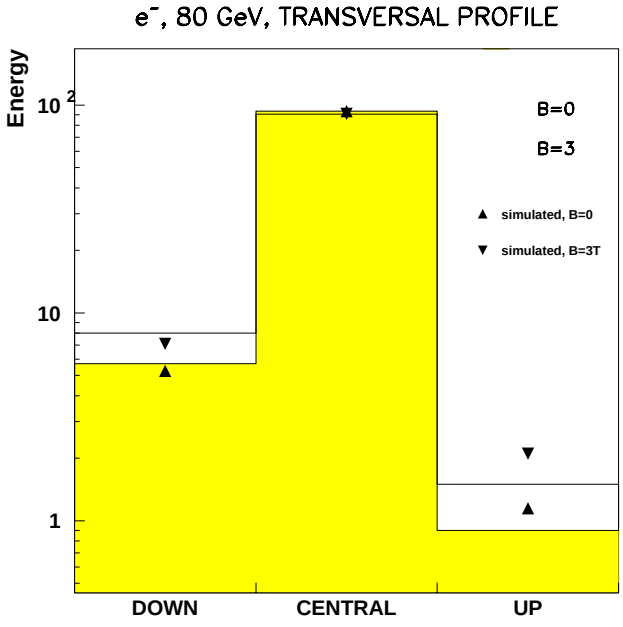

Figure 27: *Same as figure 30, in direction perpendicular to the field, with and without magnetic field. Also shown are Monte Carlo predictions with and without field.*

The Shashlik position resolution is presented in figure 28 without and with magnetic field, as a function of the distance to tower center. The resolution obtained with the field on is found to be slightly better than with field off, due to the modification of the energy sharing between central and next to central towers. In case of data with the preshower in front, the distance between preshower and Shashlik was also kept small to avoid any shower leakage due to low energy electron / positrons which are swept away due to strong magnetic field.

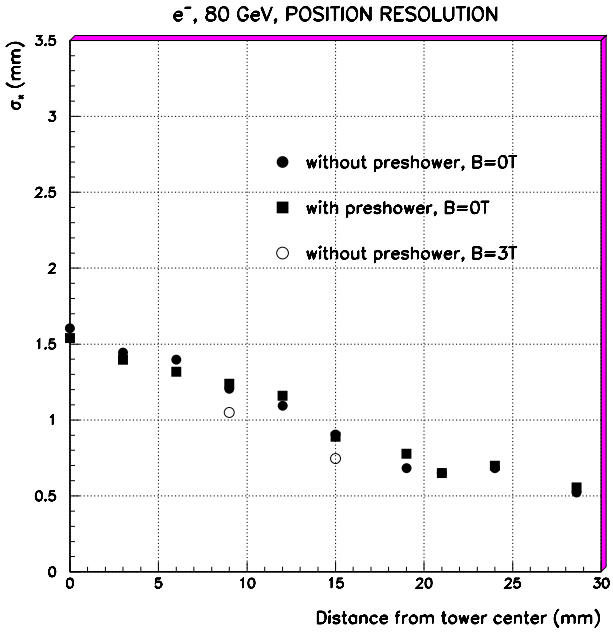

Figure 28: *Position resolution in the Shashlik calorimeter for 80 GeV electrons as a function of the distance to tower center with and without magnetic field.*

2.4.4. Effect of B field on energy resolution

The energy resolution of the calorimeter is generally parametrized as,

$$\frac{\sigma_E}{E} = \frac{a}{\sqrt{E}} \oplus \frac{b}{E} \oplus c$$

where the parameter *a* defines the stochastic term, *b* the noise term, *c* the constant term, and E is the energy in GeV. Here we have a terms proportional to ln E due to shower leakage since Shashlik is long enough (25.5 X_0). Since we had large statistics sample (several tens of thousands of events per energy point), the systematic error dominates.

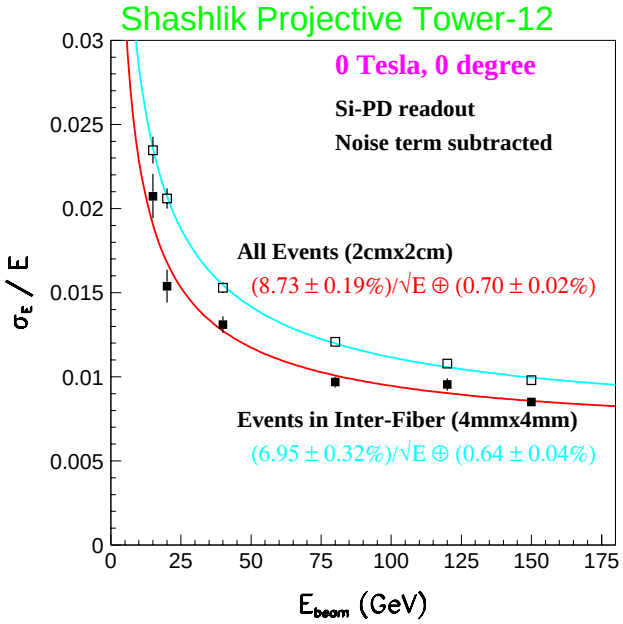

Figure 29: *Energy resolution of Shashlik alone in 0 T.*

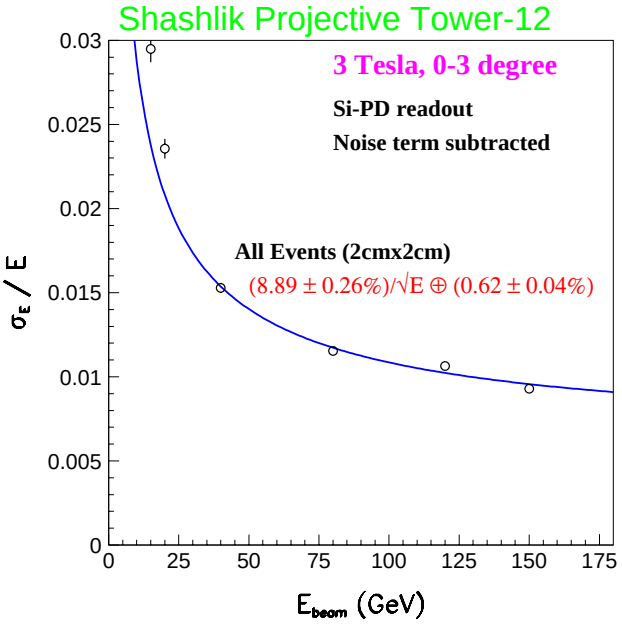

Figure 30: *Energy resolution of Shashlik alone in 3 T.*

The noise term has been measured using the pedestal data and fixed when fitting the energy resolution. No significant correlated noise between readout channels has been observed. The signals were readout with pre-amplifier / Shaper plus active post-amplifier and the noise was found to be 170 MeV per channel.
Figures 29 and 30 show the energy resolution of the Shashlik calorimeter without and with magnetic field. In both

cases a constant term of 0.7% for a 2 x 2 cm^2 area has been obtained. The stochastic term is 8.8%.

2.4.5. Energy resolution of Shashlik+Preshower

Data with an active preshower in front of the calorimeter are shown in figure 31. The constant term remains practically the same. Note however that the data analysed in the magnetic field were not identical to those for Shashlik alone due to gaps between silicon wafers. Data correspond to a 6 x 10 mm^2 area, thus giving slightly better resolution when compared with Shashlik alone because of residual non-uniformity.

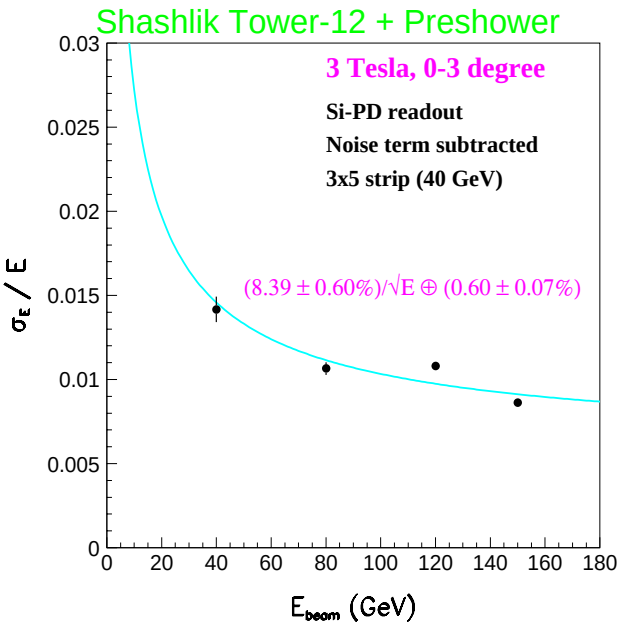

Figure 31: *Energy resolution of Shashlik plus preshower in 3 Tesla.*

2.5. Energy resolution of the calorimeter

In this section, the results with H4 beam data for newly constructed Shashlik prototypes (6 x 6 NEW IHEP matrix, Fig. 3) will be described. All the towers were tilted by 3 degree in one direction and projective in the other direction. For energy resolution study, events with 'wide beam' (2x2 cm^2) were analysed and a lateral non-uniformity correction was applied to extract the intrinsic Shashlik energy resolution.

2.5.1. Energy resolution of bare Shashlik

To study the energy resolution the signals were summed over 9 towers and the data used were the events in a 2x2 cm^2 area with lateral non-uniformity correction described in section 2.3.

For the noise estimation, the pedestal data should have been used, but the pedestal values for high gain were too small (about 20 ADC counts) which permitted the signal to swing into negative ADC value, hence making impossible the noise estimation. Since we had 8 different energy points, the noise term was fitted simultaneously with the stochastic and constant term.

A summary of the Shashlik energy resolution is shown in figure 32 for four towers T-15, 16, 21 and 22. Tower-21 had a special geometry in that the WLS fibres were also projective. The average resolution for the 4 towers is:

$$\frac{\sigma_E}{E} = \frac{8.1\%}{\sqrt{E}} \oplus \frac{0.330}{E} \oplus 0.5\%$$

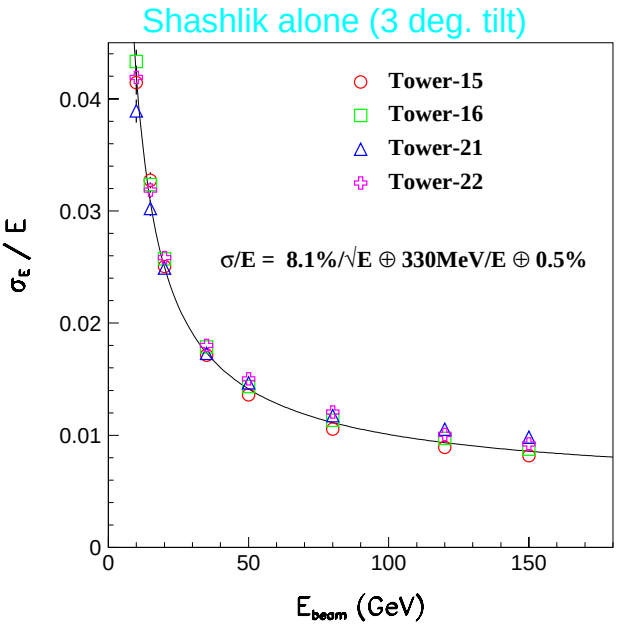

Figure 32: *Energy resolution of new Shashlik prototype.*

The results of a Monte Carlo simulation with the detailed test beam geometry are shown in figure 33 for various thickness of material in front of the calorimeter.

The Monte Carlo simulation including the saturation effect in the scintillator assumes an infinite calorimeter to study the stochastic term. With the test beam condition (~10% X_0), it predicts a 7.9% stochastic term which is consistent with the observed 8.1%. Note that with 30% X_0 material before the calorimeter, the stochastic term would exceed 9%.

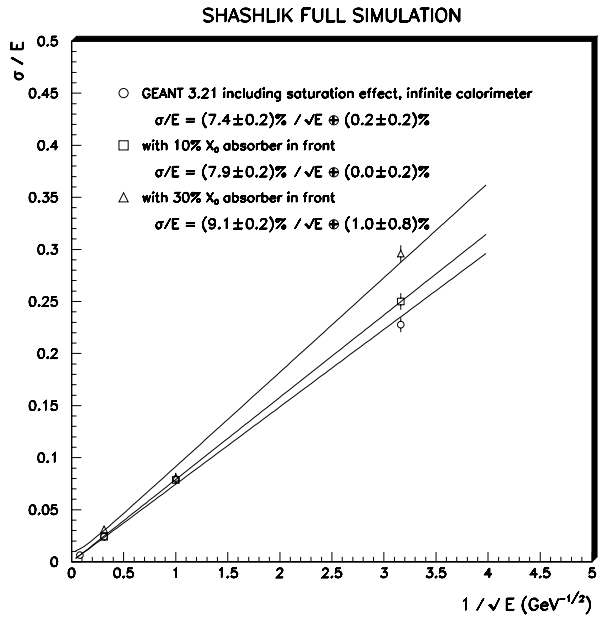

Figure 33: *Effect of absorber in front of Shashlik.*

2.5.2. Full size prototype energy resolution

For 80 and 150 GeV electron data, we have measured the energy resolution (σ/E) over the whole area of the 16 towers. Results for the 80 GeV data are shown in the figure 34.

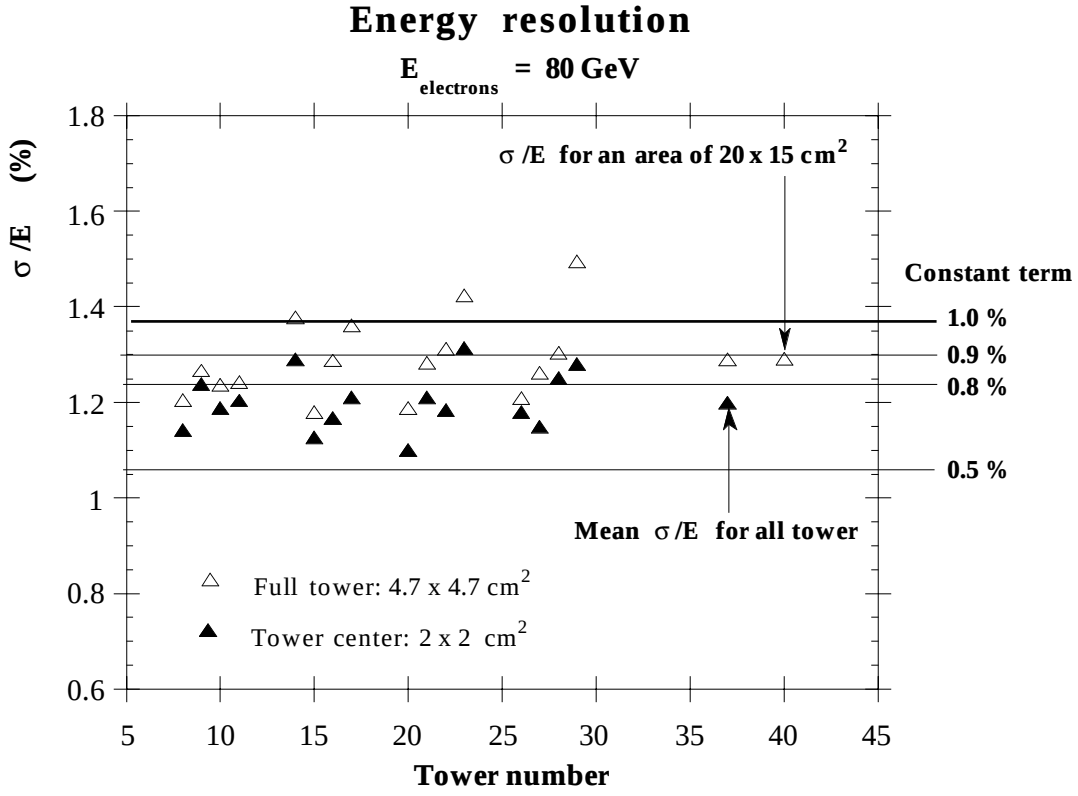

Figure 34: *Energy resolution for all 16 Shashlik towers after uniformity correction at tower center (2x2 cm^2 area) and for the full towers (4.7 x 4,7 cm^2 area) .*

One sees that the σ/E dispersion for the 16 individual towers is small and compatible with the results obtained from the energy scan data (see section 2.5) performed on the tower center (2 x 2 cm^2 area). When all data are used (20 x 15 cm^2) the overall resolution is still good and compatible with the one obtained for the individual towers.

On figure 34, we have drawn lines for different values of the constant term assuming the statistical (8.1%) and noise (.33 GeV) terms measured at the tower center. One sees that for most of the towers the data are compatible with a constant term smaller than 1%. The averaged on 16 towers mean data corresponds to a constant term of 0.8%. Figures 35 and 36 shows for the 16 towers covering an area of about 20 x 15 cm^2 the obtained energy spectra for 80 and 150 GeV electrons. One measures a σ/E = 1.05 % for the data at 150 GeV.

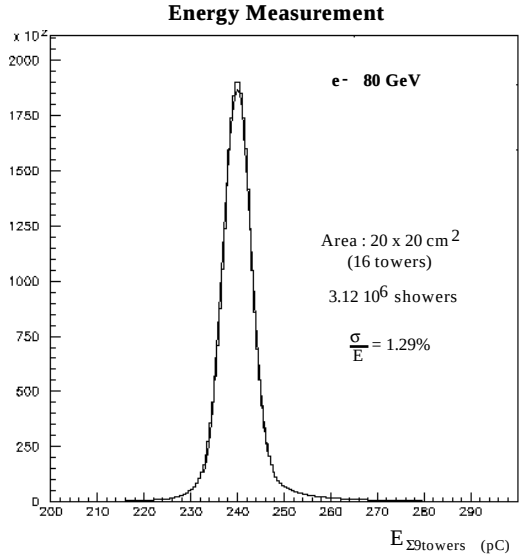

Figure 35: *Measured energy by a Shashlik calorimeter. Data have been used from the 16 towers exposed to 80 GeV electron beam (20x15cm^2 area) .*

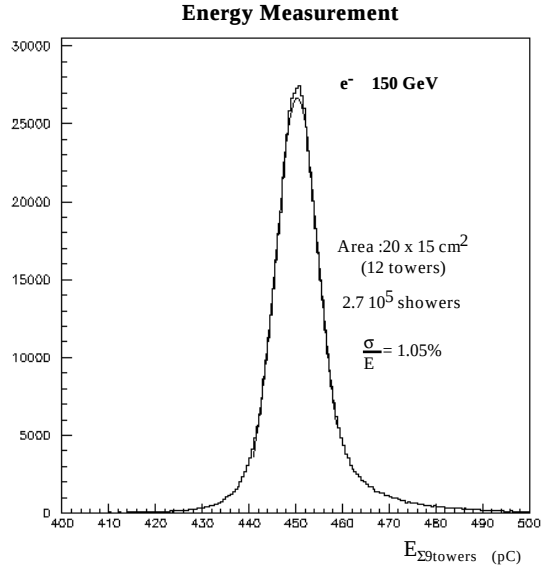

Figure 36: *Measured energy by a Shashlik calorimeter. Data have been used from the 16 towers exposed to 150 GeV electron beam(20x15cm^2 area) .*

2.5.3. Energy resolution of Shashlik+Preshower

When the preshower detector is inserted in front of the calorimeter, a fraction of the energy is lost in the $3X_0$ absorber and must be corrected for, using the energy deposited in the Silicon planes. One would therefore expect that the electron energy could be simply obtained by the expression:

$$E_{beam} = \alpha E_{ps1} + \beta E_{ps2} + E_{sh}$$

where $E_{ps1,ps2}$ are the energies measured in the 2 silicon layers (figure 37), E_{sh} is the energy measured in the Shashlik calorimeter, using the calibration obtained *without* preshower, and α and β are suitable coefficients. However, the estimate of the total energy is complicated by additional effects :

i) Some of the low energy particles present in the shower after the preshower radiator are absorbed in the structural material in front of the tower. While in the case of the bare Shashlik, only 1% of the energy is lost in this material (Fig 38), this effect increases when the preshower is inserted and depends strongly on the incident electron energy.

ii) It is well known that the sampling fraction (ratio of light in the scintillator to the energy deposited in the proceeding calorimeter absorber plate) varies along the shower depth. It is higher in the early shower development. As a consequence, the same incident energy in the calorimeter will produce different light output, depending on the presence or absence of the preshower.

iii) The compensation between light collection and fibre attenuation depends on the longitudinal profile and is therefore different in the case where a preshower is inserted.

iv) finally, the measured signal is more sensitive to any non-linearity of the calorimeter read-out in the case of a degraded shower than for a single incident electrons.

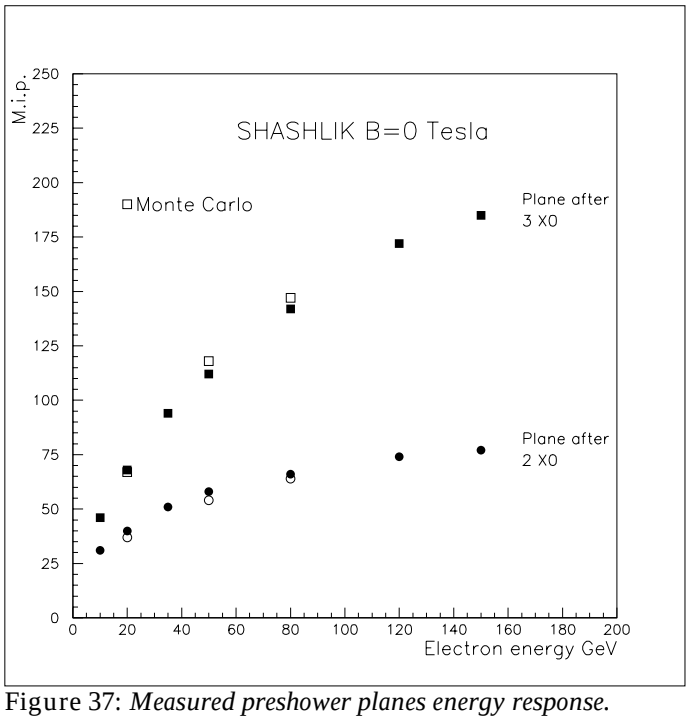

Figure 37: *Measured preshower planes energy response.*

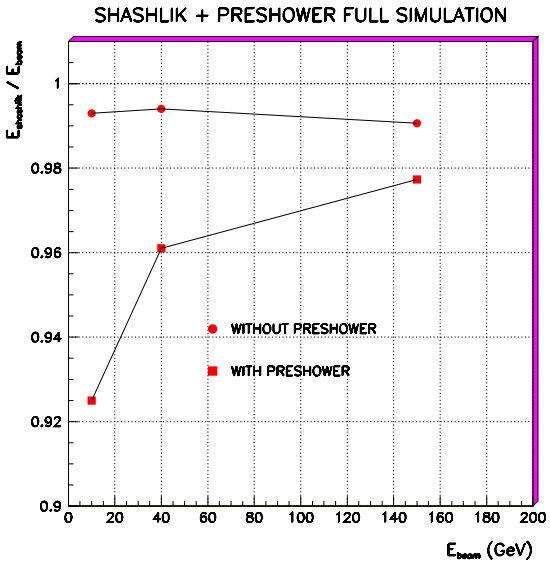

Figure 38: *Effect of preshower on average Shashlik energy.*

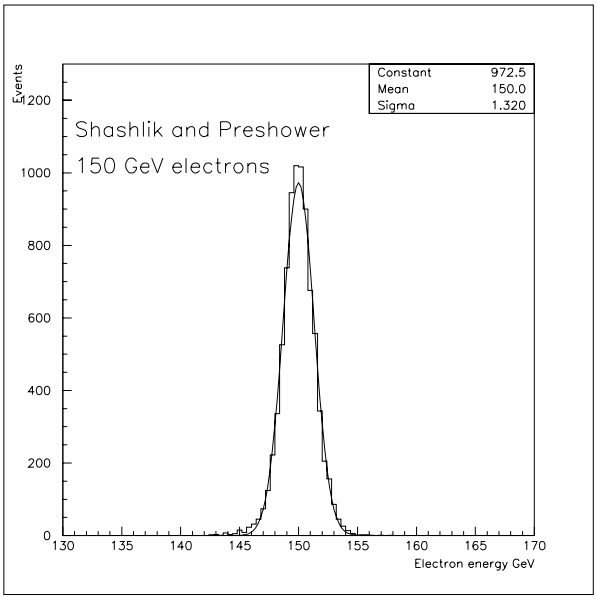

Figure 39: *Reconstructed energy in Shashlik and preshower for electron 150 GeV for Tower-15. The solid curve is the result of fit with gaussian function.*

For all these reasons, it is not possible to determine in a absolute way the energy deposited in the Shashlik calorimeter using the calibration obtained without preshower. We have therefore introduced a 3rd parameter γ and we have obtained the energy resolution by minimising

$$\chi^2 = \sum_{event}(E_{beam} - \alpha E_{ps1} - \beta E_{ps2} - \gamma E_{sh})$$

Similar results could be obtained by minimising the anti correlation curve between preshower energy and Shashlik energy, namely without knowing the beam energy. One finds that the parameters α and β are practically energy independent. The reconstructed energy measured with this method is shown in figure 39 for 150 GeV electrons. The curve fits well a gaussian, and no non-gaussian tail due to shower leakage or nuclear counting effect in silicon photodiode is seen. The results on the energy resolution are shown in figure 40 for tower T-15, 16, 21 and 22. The energy resolution of the calorimeter is fully recovered above 40 GeV if one compares these results with those for Shashlik alone. The average resolution is,

$$\frac{\sigma_E}{E} = \frac{8.5\%}{\sqrt{E}} \oplus \frac{0.330}{E} \oplus 0.5\%$$

where the stochastic term is slightly worse (0.4%) than that with Shashlik alone, but the same constant term has been observed. Noise term has been fixed with that for Shashlik alone because any significant additional noise contribution is not expected from preshower system. These results are in good agreement with Monte Carlo simulation.

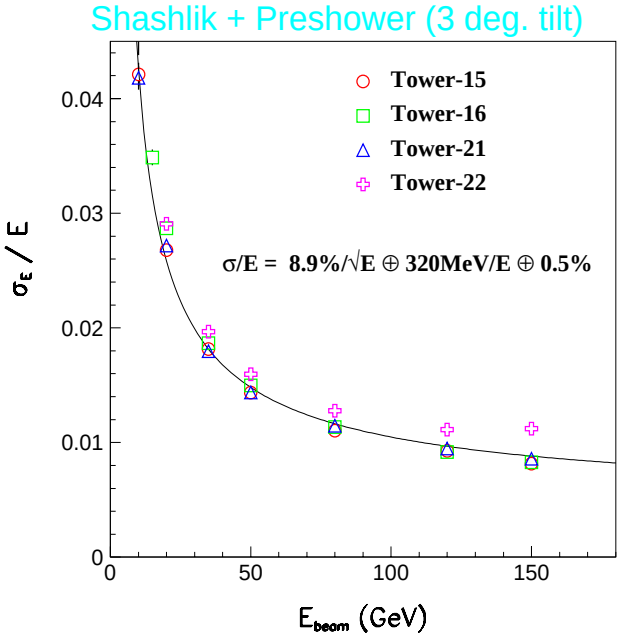

Figure 40: *Energy resolution of new Shashlik + preshower.*

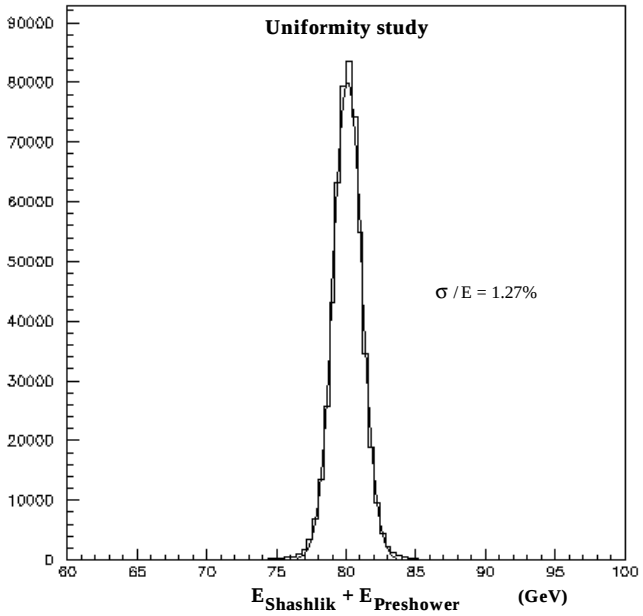

Figure 41: *Shashlik + preshower measured energy for 80 GeV electrons hitting towers 15, 16, 21 and 22.*

Using the uniformity corrections defined in section 2.3 and the weighting factors for the preshower and Shashlik towers, one obtains for all the data recorded in towers 15, 16, 21 and 22, the energy distribution shown in figure 41. The energy resolution is equivalent to the one we obtained for the bare Shashlik.

2.6. Shashlik calorimeter and Preshower position resolution

For the H-->γγ process at high luminosity the measurement of the angle of emission of the photons is required. In order to reconstruct this angle the photon shower position has to be measured at two depth in the electromagnetic calorimeter. In the CMS design, this is accomplished by introducing a preshower detector. The two planes of silicon strip placed after $2X_0$ and $1X_0$ absorber give the x and y of a first point, the second point is obtained from the shower barycenter in the calorimeter itself.

Figure 42 shows the position resolution of the preshower when 80 GeV electrons hit the detector. A resolution of ≈300μm, after unfolding of the beam chamber contribution, is measured. The resolution varies as function of the energy. It was found to follow:

$$\sigma_x(\mathrm{mm}) = \frac{2}{\sqrt{E}} + .2$$

where E is in GeV. Previous results obtained with the nonet prototypes and old projective towers are reported in reference [2.6]

Figure 43 shows the measured calorimeter position resolution for the NEW IHEP towers. The mean result for the tilted direction is as foreseen slightly worse than the one for the non tilted direction.

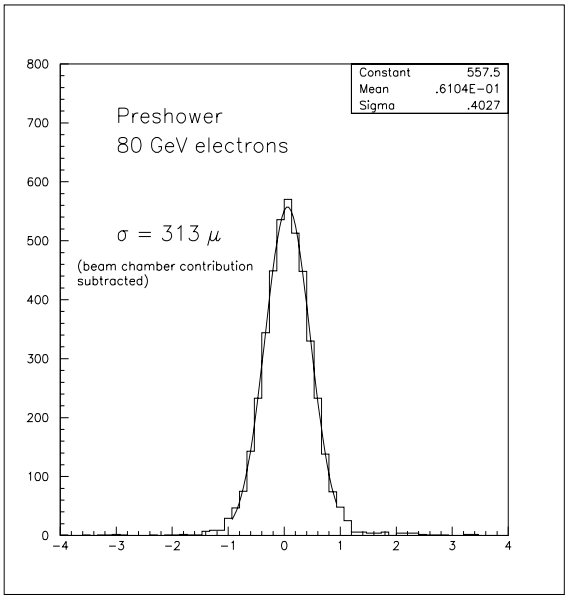

Figure 42: *Preshower position resolution for 80 GeV electrons*

Figure 44 gives the Shashlik calorimeter shower position resolution at tower center (T22) as function of the electron energy. Also shown for 80 GeV e^- the resolution for an area covering the full tower 22 and two half adjacent towers (T21 and T23).

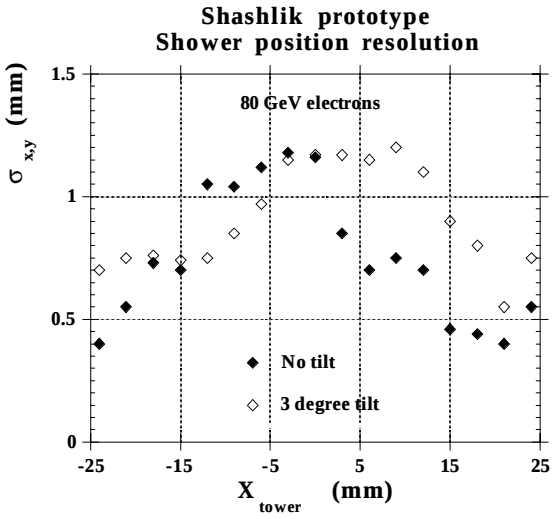

Figure 43: *Shashlik shower position resolution for the non tilted and the 3 degree tilted direction.*

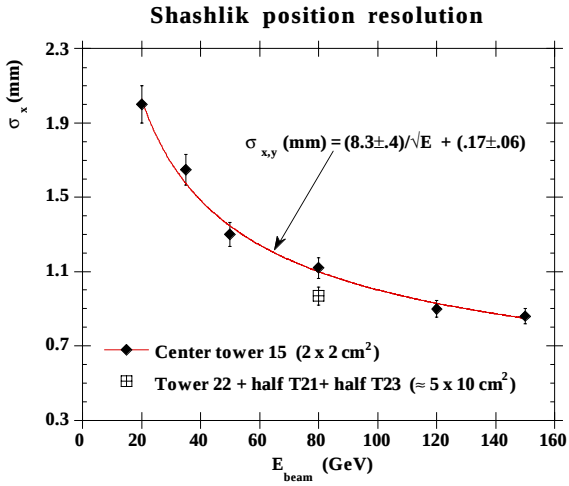

Figure 44: *Shashlik calorimeter shower position resolution*

2.7. Angular resolution

With the preshower and Shashlik tower position resolutions, assuming that the shower barycenter is located at the shower average, one can estimate the angular resolution for the combined detector.
Figure 45 shows the dependence of the angular resolution as function of the electron energy at the tower center. Our data fit:

$$\sigma_\vartheta = \frac{70 mrad}{\sqrt{E}}$$

The result is very dependent on the lever arm between the 2 coordinate measurements. We have used at 80 GeV a lever arm of 14.4 cm.
We have also given a measurement performed with 80 GeV electron on an area covering two half towers (tower 21 and 23) and completely the tower 22. The mean angular resolution is 6.5 mrad

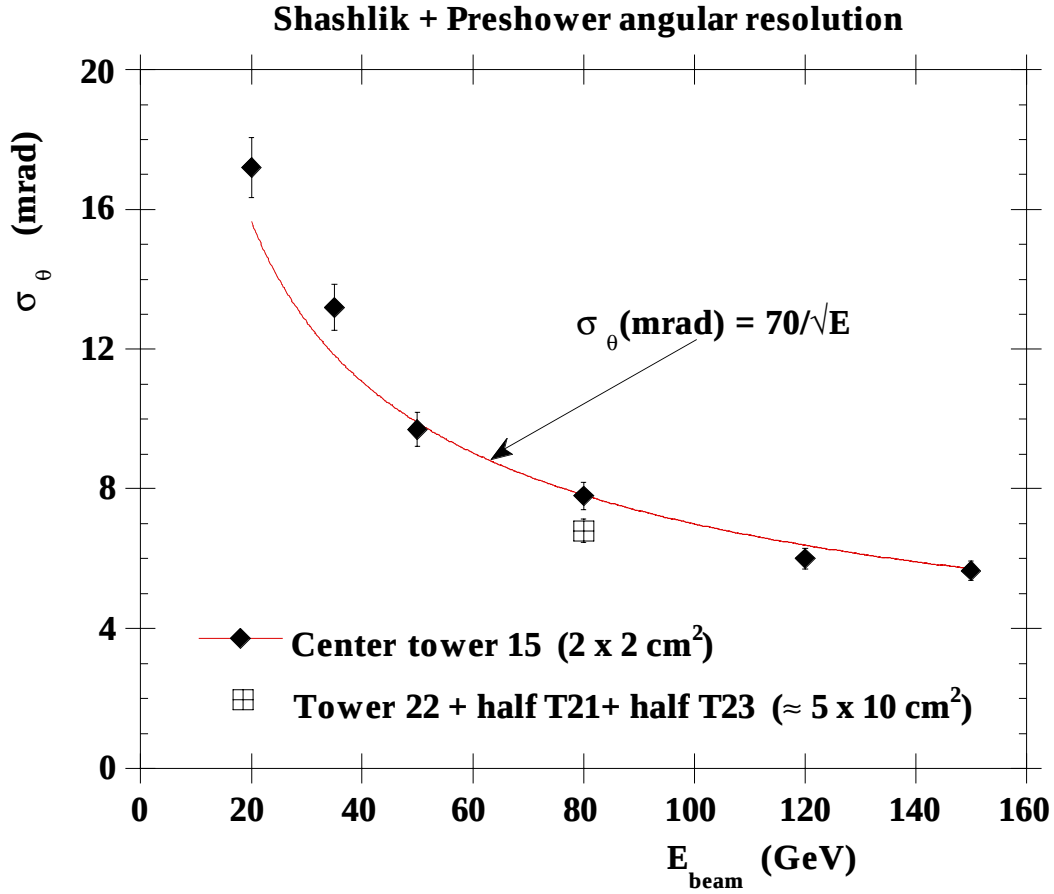

Figure 45: *Shashlik + Preshower angular resolution*

2.8. Performance of a multi-bundle Shashlik Calorimeter.

2.8.1. Introduction.

The main advantage of a Shashlik type calorimeter is its much lower cost in comparison with a homogeneous (total absorption) calorimeter. Its cost is essentially defined by high precision machining of lead and scintillator tiles, necessary for good hermeticity and uniformity of the detector. It is therefore dependent on the number of towers needed. This implies construction of towers with a size as large as possible. On the other hand, the calorimeter cell size should be small enough to provide the required spatial resolution and low energy pile-up. As a compromise, the following multi-bundle tower design was proposed and tested.

2.8.2. Multi-bundle tower design.

Among the 'Shashlik' prototype projective towers (OLD_PROJECTIVE) tested at CERN two towers were manufactured as shown in the figures 46, 47 and 48. The fibres collected in bunches, share the light signal from calorimeter tiles, leading to two and three readout channels in one single tower. The separation of fibres is done in one direction only to satisfy the requirement of more precise coordinate measurement in pseudorapidity.

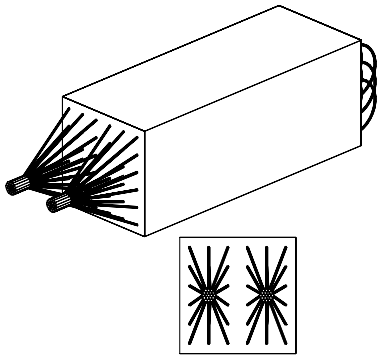

Figure 46: *Two-bundle tower*

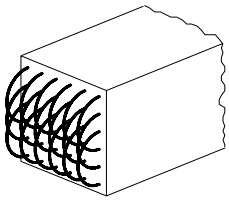

Figure 47: *Front view of the tower*

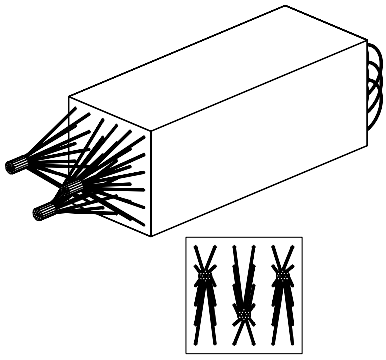

Figure 48: *Three-bundle tower*

Since all the fibres in one tower collect light from the same scintillator tiles, a point-like light source will give a signal in all channels. This may be considered as a cross-talk between channels. However its value depends on the light source position so it can be used for coordinate measurements. As a drawback, the pile-up noise may increase. More simulation studies are still necessary to define the optimal tower dimension for the LHC experimental conditions. A Monte-Carlo study of the spatial resolution and two shower separation for non-projective tower was done in the work reported in reference [2.14]. The tested towers were projective with square cross-section. The dimensions of front and rear faces are respectively 52.5 x 52.5 mm^2 and 64 x 64 mm^2. The fibres placed in a 6 x 6 matrix with a pitch of 9.5 mm, run parallel to each other and to the tower axis. The three-bundle tower was equipped with Y-7 fibres while the two-bundle one had K-27 fibres .

2.8.3. Experimental set-up.

The program of test measurements was performed in the SPS H2 test beam at CERN. It consisted of a position scan with 40 GeV electrons beam in the horizontal plane and at the middle of the tower. The tower to be tested was situated between two towers as shown on the figure 49. The tower axis was parallel to the beam. Beam particle coordinate was measured by the beam chamber with an accuracy of 300 μm. The readout system was the same as for the single bundle tower [2.15]. The electronic noise for 3-bundle tower was equal to 130 MeV per readout channel. For the 2-bundle tower it was about 170 MeV per channel.

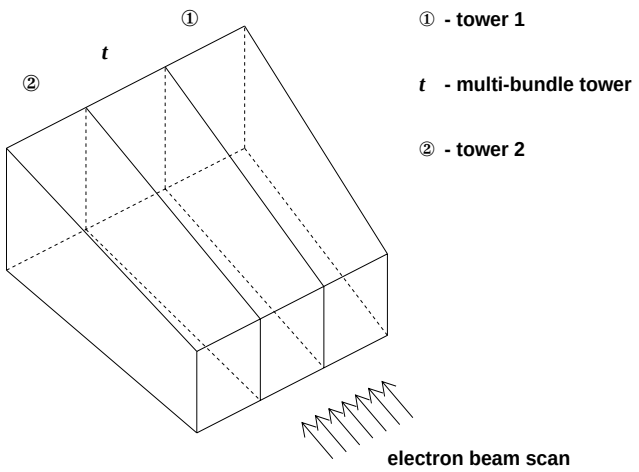

Figure 49: *Experimental setup.*

2.8.4. Experimental data and method.

2.8.4.1. Channels intercalibration.

The average response of the multi-bundle tower channels are shown on the figures 50 and 51 for a transverse position scan of the tower with a 40 GeV electron beam. For the 2-bundle tower, the calibration requires that the integrals of both channel responses over the tower transverse coordinate are equal. For the 3-bundle tower the left and the right channels are intercalibrated in the same way. The central channel was tuned to minimise the lateral non-uniformity of the tower. The total response after calibration is uniform within ±1 %.

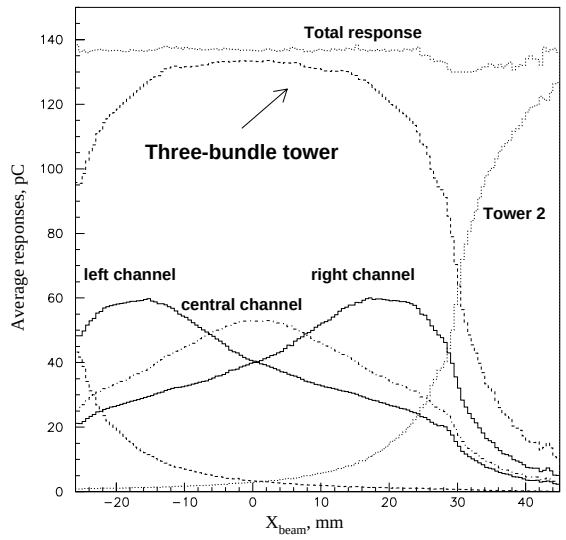

Figure 50: *Three-bundle tower channel responses.*

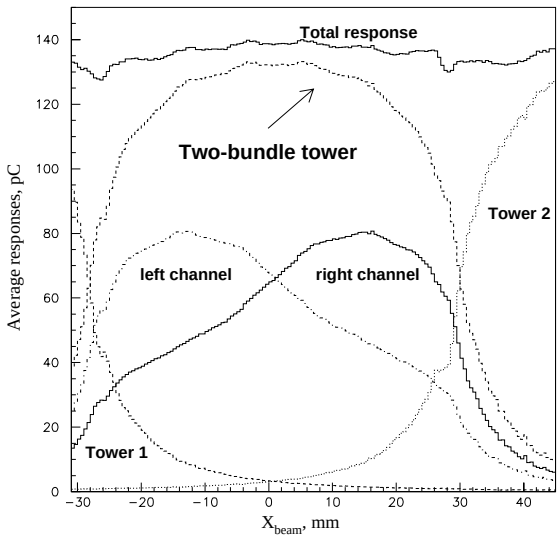

Figure 51: *Two-bundle tower channel responses*

2.8.4.2. Self-correction of fibre effect in multi-bundle tower.

Figure 52 shows the amplitude of each channel of the 3-bundle tower vs. the transverse coordinate when events are selected in a slice (±1.5mm) around the fibres. Close to a fibre the response of the channel containing these fibres is distorted.

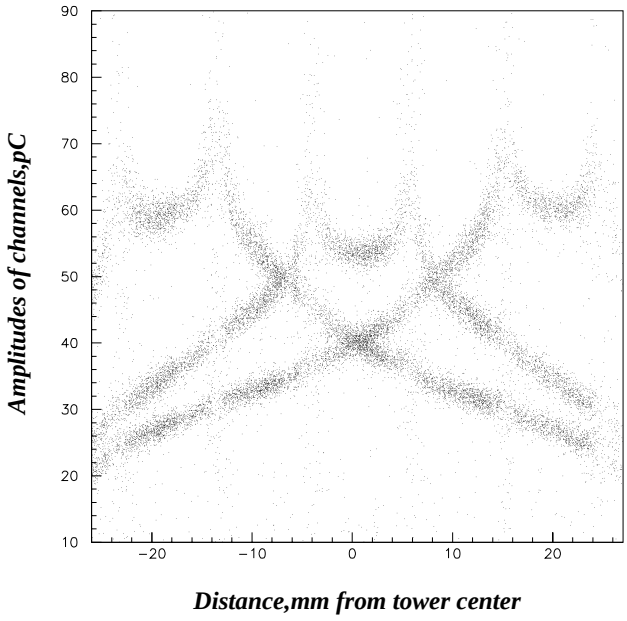

Figure 52: *3-bundle tower responses superimposed for data across fibres regions*

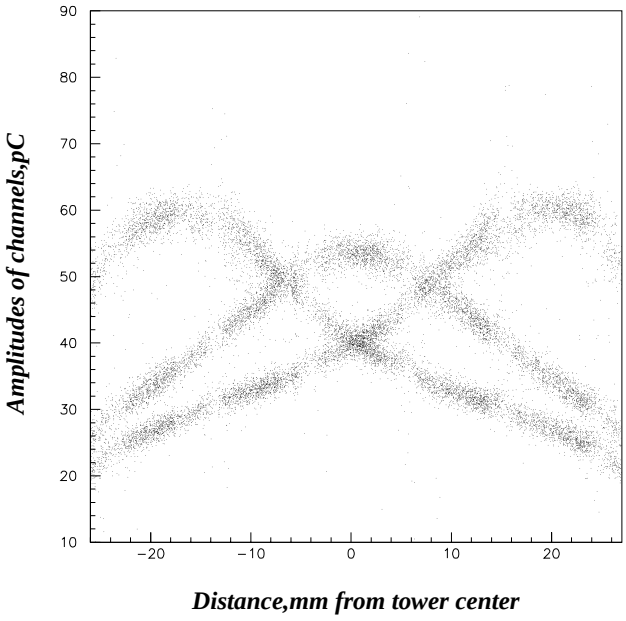

Figure 53: *3-bundle tower channel responses after correction.*

As the signal in the other channels is not perturbed, they can be used to correct for such distortions using the redundancy of multi-bundle readout based on the strong channel to channel correlation[2.5]. The correlation

functions are defined using the shower shape and the light collection conditions. It can be shown that they are practically independent of the shower energy. The corrected channel responses are shown on the figure 53.

2.8.4.3. Shower spatial resolution.

The electromagnetic shower position in a calorimeter can be determined from the response of adjacent towers. The cross-talk between readout channels in the case of multi-bundle tower leads to a distortion of the shower shape. This makes the analysis of spatial resolution more complicated than for a tower with a single readout.

The details of the method we used for the reconstruction of the shower position were described in reference [2.5]. The improvement in the spatial resolution achieved with the multi-bundle readout is shown on the figure 54. For comparison the resolution obtained for a single-bundle tower with and without electronics noise is also shown. The mean value of the spatial resolution in the 2-bundle tower is 830±140 μm. The contribution of calorimeter itself to the spatial resolution after unfolding of the electronics noise contribution (330 μm) and of the beam chambers resolution (300 μm) is 690±125 μm. For the 3-bundle tower the mean value of the spatial resolution is 760±125 μm including the electronical noise (290 μm) and beam chambers contributions. The contribution of the calorimeter itself is 620±130 μm.

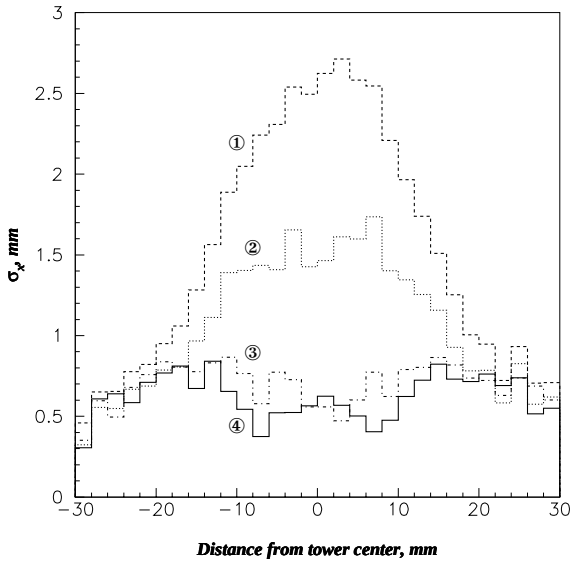

Figure 54: *Spatial resolution vs. x_{beam} coordinate. (1) 2-bundle tower if only the sum of amplitudes is used. (2) The same as (1), but electronics noise and beam chamber resolution are subtracted. (3) 2-bundle tower. (4) 3-bundle tower.*

2.8.5. Recovery of dead channel.

If the channel to channel correlation functions are known, a missing channel signal can be restored by the use of the adjacent one. This improves the calorimeter reliability, which is important for an LHC experiment which has to run over 10 years. We have found [2.15] that in the case of a 2-bundle tower the dead channel can be restored with a precision of better than 2 GeV at 40 GeV. The spatial resolution for a tower with one dead channel, is the same as for a single bundle tower. The precision of recovering the right-hand or the left-hand missing signal in the case of a 3-bundle tower is better than 1 GeV. For the central channel it is of about 300 MeV. The spatial resolution with a dead central channel is not really changed. In all cases for our data the precision of recovering a dead channel response was mainly dominated by the electronics noise.

2.8.6. Two -shower separation.

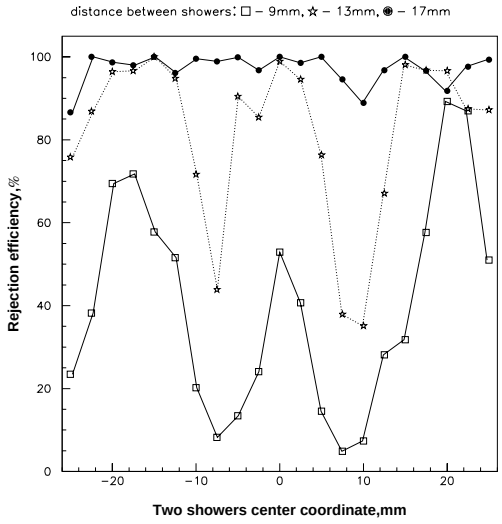

Figure 55: *The rejection efficiency for double shower events for a 3-bundle tower for events for which the single shower event acceptance is larger than 98 %*

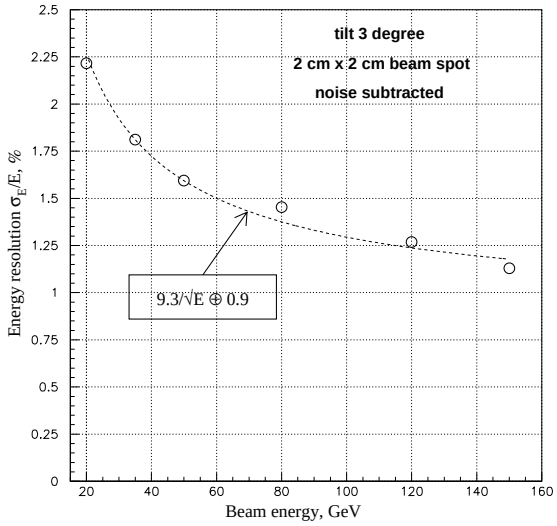

Figure 56: *The energy resolution for a 3-bundle tower.*

The redundancy in tower multi-bundle readout allows the rejection of double shower events. For this we used the same methods as for 'fibres' effect correction. We simulated a double shower events by taking the sum of two single showers responses. Thus, the electronic noise was also taken twice. The separation efficiency as function of the distance between the centers of gravity of two showers is shown on figure 55.

2.8.7. Energy resolution.

The energy resolution study for the 3-bundle tower was measured in the SPS-H4 test beam at CERN. The tower studied was installed inside a matrix of 4 x 4 single bundle towers. The calorimeter was tilted by 3 degree with respect to the beam direction in the horizontal plane. For the energy measurements we used the total response of 9 towers. The beam spot size was 2x2 cm^2. We applied only a small correction of the total response nonuniformity around the fibres position in the vertical (non tilted) direction. The result is shown on the figure 56. It is compatible with the one obtained for a single readout tower.

2.8.8. Conclusion.

Our experimental results show that:
• the spatial resolution at the tower center in multi-bundle towers is improved by a factor of 2-3 compared with the same type of tower equipped with a single channel readout.
• the lateral uniformity of the energy response in a 3-bundle tower is improved compared with towers equipped with one or two bundles.
• the correlation of channel response in multi-bundle tower provides a possibility to correct the calorimeter response in the fibre vicinity as well as for the nuclear counter effect due to the Si-photodiode.
• the reliability of the calorimeter performance as well as the two-shower separation are also improved by multi-bundle design.
• all the performances mentioned above were mainly limited by electronics noise and will be improved in the near future.

2.9. The SPAKEBAB prototype

To estimate the best possible energy resolution of a Shashlik type calorimeter, two very fine sampling calorimeters , built at Texas Tech University and University of California San Diego, were tested in the H4 Beam. The calorimeters consist of a stack of very thin lead and scintillator plates which have no physical boundaries between the readout cells (Fig. 57) . The first prototype contained 183 0.89 mm thick lead plates, while the second had 278 plates of 0.64 mm thickness.

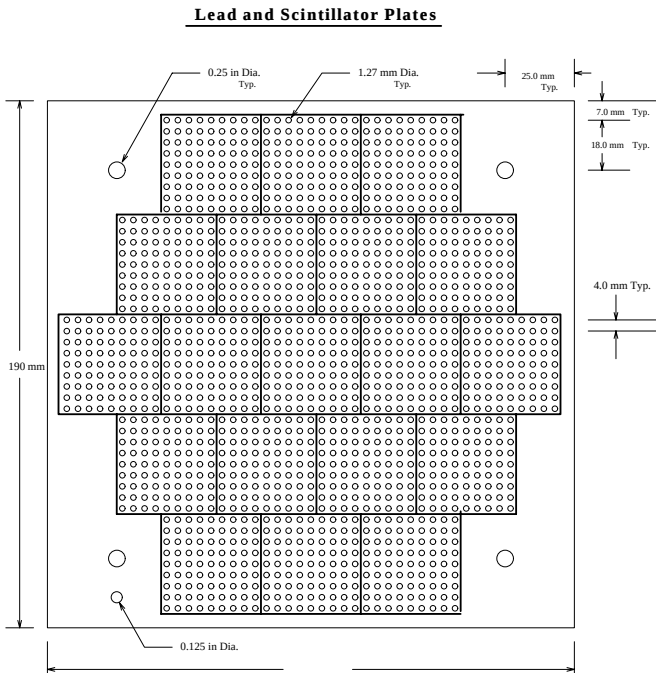

Figure 57: *Spakebab geometry and fibres arrangement.*

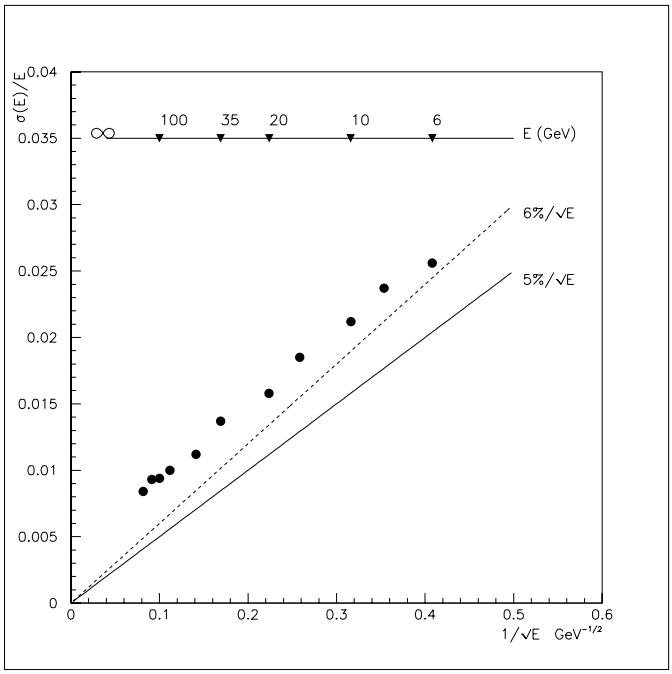

Figure 58: *Spakebab measured energy resolution.*

The readout "towers" are simply built by bundling together 9x9 square matrices of 81 fibres, coupled to a 3/4 inch PMT. The resolution obtained with the 0.64 mm prototype is shown on Fig . 58. The stochastic term is 5.5 to 6%/√E . The constant term of 0.7% is mainly accounted (as shown by EGS simulations) by the WLS fibre attenuation length, and could be drastically reduced by mirroring the end of the fibres. The spatial non uniformity is better than +-0.6% over a 3x3 cm^2 area. Since no physical boundary exists between the readout cells, there is no non-

uniformity when crossing or nearing a boundary. The cross talk from one readout cell to the adjacent one is small, and can be parametrized into an effective Moliere radius by increasing it from 2.6 cm to 3.6 cm.
More details can be found in ref [2.16]. These still preliminary results show that excellent energy resolution can be obtained with modest sampling fractions and hence very compact calorimeters.

2.10. Radiation damage for the CMS Shashlik electromagnetic calorimeter

2.10.1. CMS Environment

The LHC accelerator will produce a very high flux of charged and neutral particles due to the high luminosity and the large inelastic, non-diffractive pp cross-section of about 70 mb.
Accurate simulation of the radiation environment is not simple due to uncertainties in the cross-section at 14 TeV cms energy, and the exact composition of the events. Our most recent analysis [2.17] uses DTUJET which predicts between 10% and 20% higher neutron and photon fluxes than earlier simulations. The radiation dose from electromagnetic energy deposited in the CMS barrel calorimeter over a ten year period varies from about 0.2 Mrad, at $\eta = 0.0$, to 1 Mrad at $\eta = 1.5$ The neutron flux at the front of the calorimeter is predicted to be about 300 $kHz.cm^{-2}$ at full luminosity.

2.10.2. Effects of electromagnetic radiation

Since the CMS milestone report [1.2] further tests have been carried out on the polystyrene scintillator tiles and on a variety of WLS fibres. Irradiation has generally been at rates much higher than those that will occur at the LHC (about 100 kRad/year at full luminosity at the ends of the barrel calorimeter). Typical rates on individual components, carried out at IHEP [2.18] and INR [2.19,2.20] were 6 $Rad.s^{-1}$ (for Cs^{137} and Co^{60} photons)
The Shashlik construction technique demands that we use polystyrene based scintillators and PMMA based WLS in order to maintain the significant cost advantage over dense, radiation resistant homogeneous scintillators. Recently [2.21,2.22] polystyrene scintillators have been considerably improved by the use of new fluors (such as 3HF), synthesis with significant amounts of other copolymers (e.g. 20% of styrene by weight), or the addition of anti-radiation additives such as dibutlyphthalate. It was previously reported [2.23] that a significant improvement over standard polystyrene scintillator could be obtained by using an injection moulding technique (PSM-115(A) scintillator). The most radiation resistant polystyrene based scintillator is one containing a high quantity of an anti-radiation additive, but which has standard fluors (pTP and POPOP). Such a scintillator has 95% of the light output of standard polystyrene based scintillator but it can withstand 5-10 Mrad suffering only 10-20% permanent reduction in light output. Partial annealing of damage after irradiation occurs with a time constant of about 20h.
Progress on WLS fibres has also been made, although these remain more sensitive to radiation damage. The best material (using the fluor K-27, a benzoxanthene derivative) suffers from a loss of conversion efficiency, but little decrease in attenuation length. This can be compared with the well known Y-7 fluor whose conversion efficiency is essentially unaffected by radiation, but which suffers from an enormous increase in attenuation with dose. The effect of cladding the fibres with fluorinated PMMA is to increase their radiation resistance. This effect has been confirmed in a Shashlik-like calorimeter built by Anzivino et al [2.24].

2.10.3 Effects of radiation on Shashlik performance

The effect on the performance of Shashlik modules has been studied by realistic modelling and by the irradiation of complete towers.

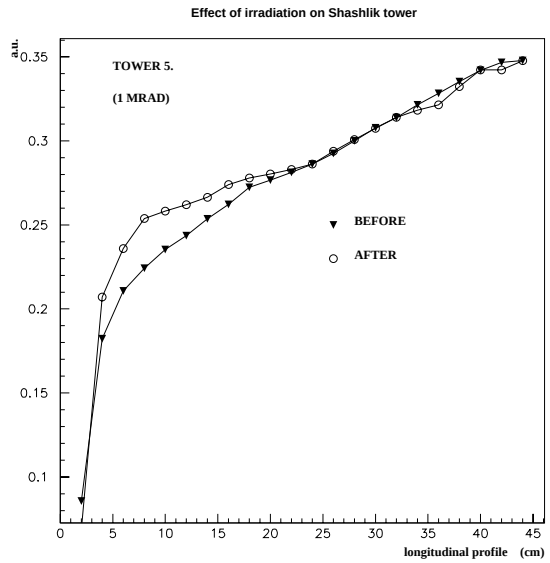

Figure 59: *Effect of an irradiation of 1 Mrad produced at LiL by 500 MeV electrons on a Shashlik tower. Longitudinal profile of the tower before and after the irradiation are shown.*

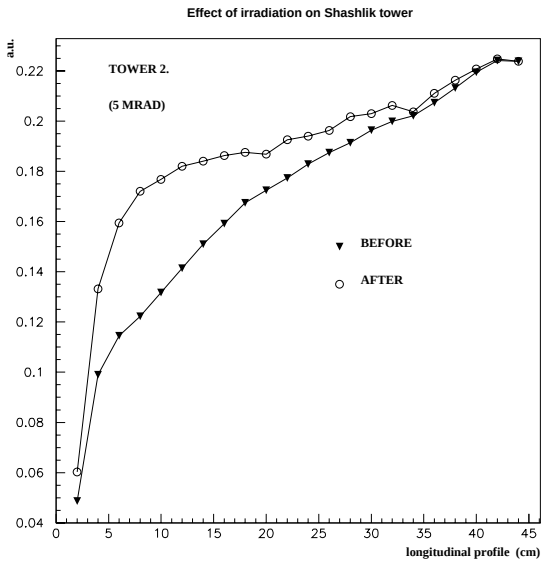

Figure 60: *Effect of an irradiation of 5 Mrad produced at LiL by 500 MeV electrons on a Shashlik tower. Longitudinal profile of the tower before and after the irradiation are shown.*

A study of the effects of radiation damage on light collection [2.25 to 2.28] shows that in addition to the overall decrease in light collected, the non-uniformity of response across a calorimeter tower increases. This leads to an increase in the contribution of the constant term to the energy resolution. Irradiation of complete Shashlik towers using the LiL injector to LEP at CERN (up to 10^9 500 MeV electrons per second) was carried out. The damage profile follows closely the shower profile and is confined to the first few radiation lengths. Figures 59 and 60 show the effects of 1 Mrad and 5 Mrad doses on the longitudinal response of the tower to ^{60}Co photons. Further tests of the energy resolution, using 150 GeV electrons, confirm that no significant effect occurs for damage up to 1 Mrad.

2.10.4. Conclusions

Developments in radiation resistant scintillators and WLS fibres have enabled the construction of Shashlik calorimeter towers which will withstand the full 10 year radiation dose in the barrel region of the CMS detector with no significant deterioration of the energy resolution. Currently it is the damage to the WLS fibres as well as the scintillator tiles that are the limiting factor in using the Shashlik calorimeter in the CMS EndCaps where the dose will reach 8 Mrad over 10 years of LHC operation. Radiation hard material has to be developed and used.

3. Preshower electronics status report

3.1. Introduction

During the last year, electronic R&D for RD36 has been dedicated to the development of the basic silicon chip components. These include a low power fast preamplifier, a large dynamic range analog memory and a radiation hard ADC. Simulations and experimental results of these prototype chips indicate that the target specification of the project is feasible in terms of dynamic range, speed, density, noise, power consumption and functionality. Improvements in the design of the preamp to enable DC coupling to the silicon detector with large leakage current and differential charge readout of the analog memory for better precision and baseline stability are under way and submission on silicon for validation is planned in 1995.

The modelling of the analog and digital signal processing including characteristics of the silicon detector before and after radiation damage, is now established and a computer model will be developed in 1995. This model will enable the prediction of the performance and the variations of the Si-preshower characteristics as a function of the temperature, bias voltage of the detector, timing uncertainty and ageing effect caused by radiation damage of the silicon detector and readout electronics.

Critical components of the Si preshower readout electronics, such as the fast preamplifier, the analog memory and the ADC have been designed and implemented in radiation hard technologies, HSOI3HD of THOMSON TCS [3.1], and in DMILL technology [3.2]. Prototype chips will be available at the beginning of 1995 to evaluate their radiation hardness characteristics.

3.2. Principle of the preshower readout chip

The principle of the proposed readout architecture of the preshower electronics is based on the previous HARP development done in the framework of RD2 [3.3] with major changes based of the following new requirements:

- the preshower granularity is matched to the detector to give 32 channels per chip.
- the maximum power dissipation of 10mW/ch to enable the construction of an acceptable cooling system and a minimum δT for the barrel.
- a simple bunch crossing identification by measuring at least the 2/3 of the SiDet charge within a sampling time period of 25 ns.
- a dynamic range of 11 bits determined by a max range of 500 MIPs and a noise less than a 1/4 of MIP.
- a radiation hardness of at least 10 Mrad and 10^{14} n/cm^2 to be compatible with the end cap environment.
- a local analog storage time of 3μs imposed by the LV1 trigger latency.

The basic preshower analog electronics channel consists of :

- *A current mode CMOS preamplifier* which conveys the SiDet charge from the high capacitance node, up to 80 pF, to the small output capacitance node, less than 1 pF.
- *A write amplifier,* i.e. a fast CMOS transconductance amplifier which integrates the output signal of the current preamplifier into the memory capacitance Cs, via the write bus during a clock period of 25 ns. This circuit acts as a charge-to-voltage sampler.
- *An analog memory* which consists of a bank of 128 capacitors Cs of 0.4 pF connected via a pair of read and write n-channel MOS switches to the write and read bus with the digital circuit which generate and control the write and read pointers.
- *A differential read amplifier* which retrieves the storage charge of Cs through the read bus. Presently, only a single ended version is implemented on silicon.
- *A fast 32 input analog multiplexer* to transfer serially analog signal to the digital to analog converter
- *A large dynamique low power ADC* capable to convert 20-40 Msample/s analog signals with a dynamic range of 12 bits at a power consumption less than 50 mW. This ADC is based on the CRIAD development [3.4] capable to convert 32 analog samples in less than 2.5μs.

The digital part which follows the analog part of the readout chip consists of a FIFO buffering data and a DSP which operates a thresholding, zero suppression, the bunch crossing identification and performs 2 algorithmic operations to extract the total charge and the timing skew.

3.3. Upgraded specifications for Barrel and End cap

The barrel and end cap have slightly different specifications due to different geometry's of the silicon detector and the different irradiation levels. Nevertheless, specifications are unique because only one chip will be used for both detectors. The barrel specifications are actually more severe than those for the end cap in terms of detector capacitance which is the double of the end cap one, and power consumption which must be minimised to keep temperature variations, close to the crystal calorimeter, as small as possible. For this reason, the power budget allocation is 10mW/ch i.e. 320 mW for a detector area of 36 cm^2 corresponding to a power density of about

100 W by m^2 of silicon detector area. This specification is particularly outstanding when one assumes the high complexity of the readout electronics channel and the dynamic range of 11 bit. For this reason, minimum power consumption has been the key criteria used in the design optimisation of the different components.

End Cap /Barrel	Nominal specs
Nb of ch/Chip	32
memory depth	128 cell 3.2μs delay
Si det capa./barrel/end cap	70/35 pF
Sampling frequency.	40 Mhz
Readout frequency.	20/40 Mhz
Analog readout time	3.2-1.6μs
Digital latency processing	32 clock cycles, 3.2-1.6μs
Noise ENC	2000 rms e+50 e/pF
Total power consump./ch	10 mW/ch
Charge Gain	5 mV/MIP
Input preamp capacitance	15 pF
Integrating time	2BC, 50 ns
Input Resistance	100 Ω
Linear range voltage swing	3.5 V (-1.5V,+2V)
Det leakage/barrel/end cap	10/30μA
Nb of cell/triggered event	3
Linearity /400MIPS	1.5%
Linearity /600MIPS	3%
Radiation hardness	10 Mrad + 10^{14}n/cm^2
Operating temperature	5-10C

Table 3. Main specifications of the preshower readout electronics

3.4. Analog and digital architecture's: pros and cons.

Two readout architecture's are presently under study:

The digital architecture performs locally on chip, digitisation, BC identification, zero suppression, and digital filtering. The transmission would be done serially via a digital optical link which can be based on a LED, laser diode or MQW used in digital mode[3.5].

Assuming a maximum channel occupancy of 10%, a trigger rate of 100 Khz, one link for 1024 ch (32xSiDet) and, a formatted word of 24 bit; the required maximum bandwidth is about 245 Mbit/s. The data rate per detector is less than 10 Mbit/s. A few hundred digital optical links are sufficient to equip the entire preshower.

The key issues of the digital architecture are the design of a Rad hard and low power on chip digital signal processor (DSP) and a Rad hard optical driver. The study of the DSP is planned for 1995. There is some hope to find an optical digital link already existing in GaAs technology (Trinquit). An alternative would be to use a Multiple Quantum Well device (MQW) of RD23 adapted for higher speed for digital signals.

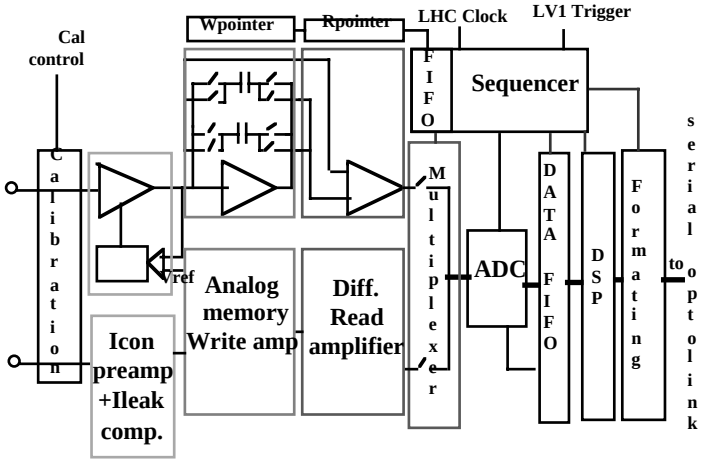

Figure 61: *Block diagram of the digital architecture*

The analog Architecture basically consists of the front end analog electronics of the digital architecture with an additional analog output interface. At the output of the analog multiplexer, the analog signal is split into 2 overlapping ranges of 7 bit by a 2 gain stage amplifier. This is done to comply with the highest possible dynamic range of the analog MQW. Consequently, each analog multiplex cycle contains 3 analog values:

- the analog signal
- the amplifier range
- the calibrated analog signal used to refresh the calibration factor of the analog link for each sample read.

The analog signal is encoded by an analog signal of 7 bits dynamic, corresponding to a swing of 0.020V to 3V at

the input of the MQW and a 2 levels analog signal for the operating range.

Clearly the advantage of the analog architecture is a lower complexity of the front end chip but at the expense of an optical link per silicon detector. For 32 channels, 3 samples/event, one range and calibration value, one gets a readout time of 4µs at 40 Mhz multiplexing frequency.

The price to pay is a much higher number of optical links, 32 times that for the digital architecture which can be a severe drawback. In addition, the operation of the analog MQW at 7 bit dynamic range is not yet proven.

Therefore, there is no compelling reason to choose presently one of these two architecture's. We propose to pursue the development of the 2 architecture's at the system level in 1995 in order to improve our understanding and better pricing of the optoelectronic components.

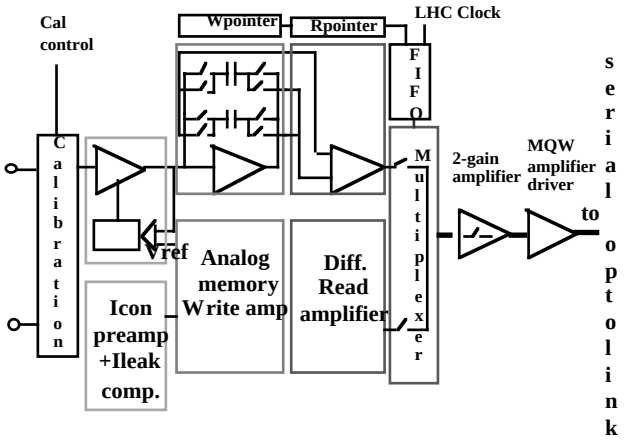

Figure 62: *Block diagram of the analogic architecture*

The R&D for the front end chip will focus on the analog front part which is common to both architecture's and a preliminary study of the DSP specific to the digital architecture.

3.5. Analog Signal processing

3.5.1. Continuous time filtering

The signal charge in the preshower silicon detector has to be precisely measured in a severe radiation environment. We can expect parameter variations due to the ageing of the radiation damage which would inevitably lead to the degradation of precision and variations of the calibration of the electronic channel. In addition, the mismatch of the capacitance of memory bank would limit the channel precision, if the channel calibration factor depends of this capacitor mismatch.

To minimise these parameter variations, the signal processing has been conceived in such a way that the calibration factor of the gain depends only on one parameter. Figure 62 shows the basic principle of the analog signal processing. The charge of the silicon detector is first amplified by the current preamplifier A_i. The input resistance of the current preamp is low enough (100Ω), to ensure a short input time constant t_i (for Ca+Cdet = 40 pF, ti = 4 ns). The output current is then integrated during the sampling period of 25 ns onto the memory capacitor Cs. The charge transfer is done through the input resistance R_{in} = 2kΩ of the write amplifier. Assuming an output capacitance C_o=2pF, the output time constant is 4 ns.

Therefore, the preamplifier stage acts as a 2 pole continuous time low-pass prefilter. The filter time constant of 4 ns is small enough to enable the charge integration in a BC of 25 ns.

On the LV1 request, the charge stored in C_s is transferred into C_{int} during the read cycle. A simple analysis of this circuit shows that only the capacitor C_{int} enters in the calibration factor of the channel. Actually, the conversion gain of the channel is:

$$G = Vout/Qdet = 1/Cint$$

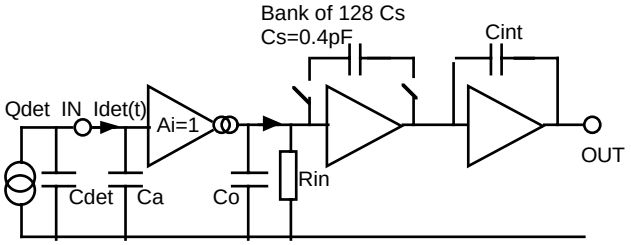

Figure 63: *The preamplifier*

3.5.2. Sampling filtering and digital signal processing

Assuming a sampling period of 25 ns, the detector signal will captured in 2 sampling periods t and t+25, with more than 80% of the charge integrated in the first period t. A third sample is recorded at the time t-25. Therefore, the total charge is obtained by the sum $Q_t + Q_{t+25} - Q_{t-25}$. The subtraction of Q_{t-25} helps to get rid of the pedestal of the base line in case of pile up and to shape the noise weighting function.

The noise calculation of the channel which associates time variant and time invariant filter cannot be easily studied analytically. The preliminary calculation of the weighting function of the entire filtering channel has been done by assuming that the prefilter is gaussian, 25 ns peaking time.

Figure 64: *Simulated noise weighting function of the entire electronic channel*

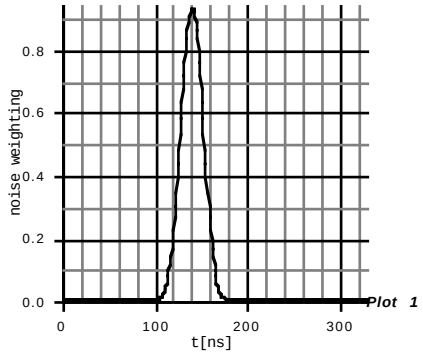

Each sample, Q_{t-25}, Q_t, Q_{t+25} have associated weighting functions, W_{t-25}, W_t, W_{t+25} which are the convolution integrals of the 3 gating signals of 25 ns with the gaussian filter. A preliminary computer simulation of the total weighting function $Wt = W_t + W_{t+25} - W_{t-25}$, is shown in figure 64. Its shape approaches closely the optimum triangular shape peaking at 25 ns. Therefore, one can consider that the filtering nearly emulates an optimum matched filter for which parallel noise from the detector leakage current and series noise from the preamplifier are minimised.

3.6. The preamplifier circuit

The preamplifier design is based on the current mode amplifier icon [3.6] to obtain high speed performance with minimum power consumption. The output branches have been cascoded by the devices MP4 and MN3 to extend the dynamic range. MOS devices MN1 and MN2 are the input devices with their load MP2 and MN2.

The bias current of the cascode branch and the input branch are controlled by a biasing branch connected to the gates of those transistor. Signal current is conveyed to the output node via the mirror MN4 and MP3.

The bias current of the cascode branch determines the maximum swing of the output current and therefore the dynamic range. The cascode bias current has been chosen at 100µA to enable a dynamic range of 400 MIP.

The bias current of the input branch determines the transconductance gmn1 and gmp1. Those value determines the input resistance $R_{in}=1/[gmn1+gmp1]$. It has been chosen a value of 250µA to obtain an input resistance of 100Ω which enable a high speed operation with an input time constant of less than 4 ns for a detector capacitance of 35 pF.

For these operating conditions, the power consumption is 2.75 mW for a supply voltage of 5 V.

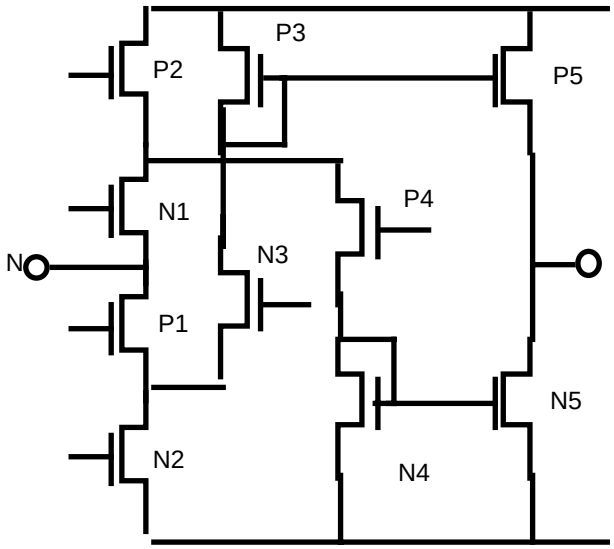

Figure 65: *MOS schematic diagram of the large dynamic range icon*

3.6.1. fc-_icon chips submission

icon design have been implemented in 3 technologies:

- MIETEC 1.5µm, prototypes are ready and testing is under way
- HSOI3HD, design has been submitted in October 94, prototypes available in April 1995.
- DMILL process, design have been submitted in May 94 and prototypes available in January 1995.

The layout of these icon chips are shown in figures 66, 67, 68.

3.6.2. Results of the MIETEC fc_icon

The icon circuit of figure 66 has been implemented in MIETEC 1.5 µm with a feedback compensation and a driver. The output voltage is an image of the output current of icon which in itself is the copy of the Si-detector signal. Simulations have been done for a bias current of 250µA and various input capacitance's. Figure 69 shows the simulated impulse response for a nominal detector capacitance of 40 pF. The gain is 1.8 mV/4 fC with an output resistor of 11KΩ giving an output time constant of 4 ns. The peaking time is about 10ns with a linear dynamic range of 1.6 pC (400MIPs)

Figure 70 shows the measured result of the impulse response for 40 fC input signal. The peaking time is 15 ns with a gain of 1.76 mV/4 fC. The slower response comes from parasitic capacitance's in the package and

measurement set up. The dynamic range has been measured as shown in Figure 71 and indicates a value of about 1,6 pC(400MIP).

Figure 66: *MIETEC 1.5 µm board.*

Figure 67: *HSOI3HD board*

Figure 68: *DMILL board.*

Figure 69: *The simulated impulse response for a nominal detector capacitance of 40 pF.*

Figure 70: *The measured result of the impulse response for 40 fC input signal.*

Figure 71: *The dynamic range*

3.6.3. Leakage current compensation

The detector leakage current compensation in the present design uses a feedback loop to balance the input DC current. This circuit adds an extra parallel noise source.

For this reason we have in development a new scheme which does not have those limitations. Figure 72 shows the principle of this new input compensation circuit. The input branch, black and the bias branch, in grey form a differential input structure with 2 current mode inputs. The normal input of the preamp which senses the detector signal and the DC detector leakage, and the bias input which senses the feedback. The additional loop amplifier forces the preamp output to be set to Vref. This implies that the current I_{dn} and I_{dp} are equal. Actually, to obtain this balance effect, if I_{leak} is added to I_{dn}, the loop forces the current in the n branch to be I_{dn}-I_{leak}. Therefore, the detector leakage current is used to bias the preamp without disturbing its DC operation and without additional noise.

The great advantage of this technique is that there is in principle no limit for the detector leakage current assuming it does not go over the bias current of 250µA.

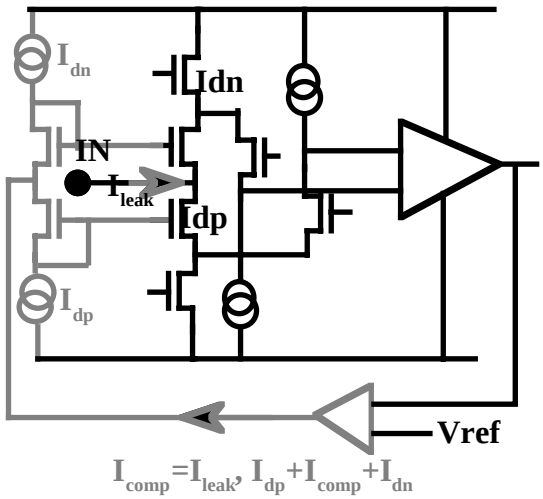

Figure 72: *Principle of the new leakage compensation for DC coupling.*

3.7. The analog memory circuit

The analog memory circuit is based on the HARP and DYN1 development[3.7].

A RD36 chip already designed and fabricated in the MIETEC 1.5µm technology is presently under test. This circuit utilises a single ended voltage amplifier for the readout of the analog memory. In the development in 1995 we propose to upgrade it by a differential charge amplifier shown in figure 73. This new sense amplifier offers the advantages to reject the common mode noise charge Q_p and to retrieve the charge Q_s which is independent of C_s as described in section 3.4.

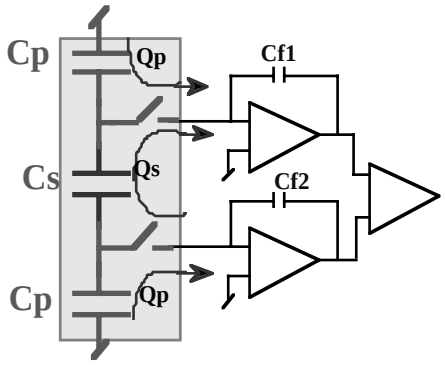

Figure 73: *Principle of the new charge readout sense amplifier*

3.8. 11 bit-ADC in Rad hard HSOI3HD CMOS-SOI process

The key component to demonstrate the feasibility of the digital architecture is the availability of a radiation hard, low power and large dynamic range ADC. This ADC has to be compatible with a radiation hard process.

During the year 1994, we have started a study in collaboration with MEAD, Lausanne, Intitut of Superior Technica (IST) Lisboa to develop a design philosophy of the ADC compatible with the radiation hardness environment of LHC experiments.

In particular we have studied the implementation of the ADC in a radiation hard process and investigated design strategies such as self calibration which makes the ADC performance quite independent of the radiation effects.

We have translated in the radiation hard process of Thomson, HSOI3HD, the 11 bit (6 bit-4 ranges) dynamic range CRIAD ADC[3.8]. SPICE simulations of the converted design, including radiation effects up to 10 Mrad, have been done on the basic cells of the ADC and have demonstrated the feasibility. The Table 4 shows the simulated performance of the rad hard ADC.

Voltage Supplies	VDD=3V, VSS=-3V
Signal input	Unpolar negative
Reference voltage	2.048V
Sub-ranges 1	0 to 64 mV
Sub-ranges 2	0 to 128 mV
Sub-ranges 3	0 to 512 mV
Sub-ranges 4	0 to 2048 mV
Number of bits	8 bit, 2 range bit, 6 data bit
Accuracy at low level	11 bit
Speed	20 Msamples/s
Power consumption	35 mW
ADC unit capacitor	150 fF
Silicon area with pads	15 mm^2

Table 4: *The simulated performance of the rad hard ADC.*

The HSOI3HD CRIAD ADC has been submitted to THOMSON for fabrication in November 1994 and prototype chips will be available for evaluation and radiation test in April 1995.

3.9. Silicon detector modelling

Study of the signal formation in the silicon detector before and after proton irradiation up to 1.1 10^{14} p/cm^2 has been done for 0° C, 10° C and room temperature. The speed of the charge collection induced by MIP have been measured in using fast current preamplifier. Results indicate that more than 90% of the charge is collected in 25 ns even after irradiation. Full depletion voltage increase of the silicon detector after irradiation and long annealing time is minimised by operating the preshower detector below 10° C. In addition, low temperature operation minimise the detector leakage current.

The modelling of the detector characteristics, such as carrier mobility and life time, effective doping concentration, has been done[3.9]. The silicon detector model under development will be capable to predict the electric characteristics of the detector signal such as speed and charge collection efficiency for different operating temperature and irradiation dose levels.

A next step of the development will be to implement in a computer programme the detector and electronic channel models. This will enable to calculate the overall performances of the preshower detector under the LHC operation.

4. Shashlik + Preshower Mechanical design

4.1. Shashlik tower mechanical tests

4.1.1. Shashlik tower mechanical parameters

The mechanical behaviour of a tower may be studied using calculations and bibliographic investigations of its components. A full understanding of the Shashlik properties need some mechanical measurements and essentially a study of the deformations and their time evolution under strain. The mechanical stability of the various kinds of prototypes has been tested. They differ in the shape, the size and the method of fabrication. The oldest prototypes were produced at Protvino. Steels rods were passed through additional holes, the pressure on the plates was balanced by the tension in the rods. In the next generation of Protvino prototypes, the rods were replaced by external stainless steel straps which were soldered to front and rear stainless steel plates. Another method to press the layers was proposed at Ecole Polytechnique: it consists of gluing an aluminium foil on the lead lateral faces. The parameters of the various prototypes are given in the table 5. The last column gives an estimation of the stress into the skins or the rods.

Type	Geometry	Front section (mm^2)	Tightener	Pressure (MPa)	Stress (MPa)
IHEP I	Non projective	47 x 47	Steel rods Φ 1 mm	.6	420
IHEP II	Projective	52 x 52	Steel strips .10mm	1.	130
IHEP III	Projective	42 x 42	Steel strips .07 mm	1.	150
Poly I	Non projective	48 x 48	Glued Al foil .05 mm	.06	14
Poly II	Projective	42 x 42	Glued Al foil .125 mm	.1	8
INR	Projective	42 x42	Glued Al foil .05 mm	.06	13

Table 5 : *Prototypes mechanical parameters.*

4.1.2. Flexibility of assembled tower

A flexion test is very simple. The tower is simply held by its ends, in horizontal position. One makes the metrology of the horizontal lateral faces. The tower deformation is measured, under its proper weight and as a function of additional weights put at the center The time evolution is also analysed in the same way.
A first set of measurements have been performed on the non projective "Poly I" towers. They have been loaded with increasing weights from 0 to 106 Newton's. The measurements are shown the figures 74 and 75.

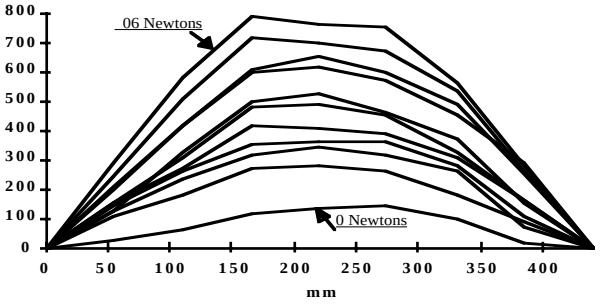

Figure 74. *Tower deformation (μm) (Poly I) for increasing load at the center.*

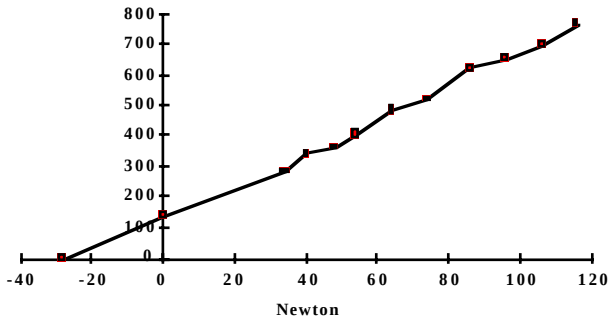

Figure 75: *Tower deformation (μm) as function of increasing load at the center.*

Figure 75 gives the variation of the tower sagitta as a function of the load. The first point is put at a negative abscissa equal to -5P / 8, were P = 45 Newton corresponding to the tower weight.
The results are very coherent and linear. The sagitta variation with respect to the load is about 6 μm per Newton. The load was applied during a very short time, after relaxation a residual deformation was observed, (<10 %). To study the mechanical stability, the time evolution of the loaded towers was studied. After several days a very large permanent deformation occurred increasing with time.
In order to have a better understanding of the phenomena, the time evolution of the shape of a "Poly II" tower was studied, without any additional load. Results are displayed on figures 76 and 77. The behaviour is similar to a creep. During the first week the additional permanent deformation was about 70 % of the initial one. Afterwards the deformation continues linearly with the time at the level of 1 % per 15 days.

Figure 76 *Tower deformation (μm) (Poly II). Evolution of the deformation with the time.*

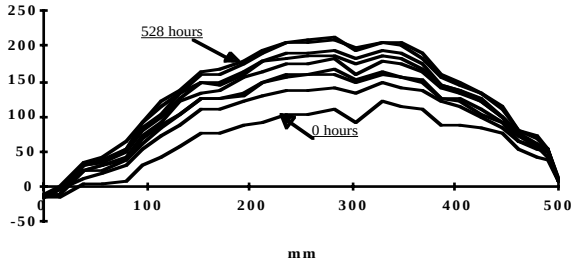

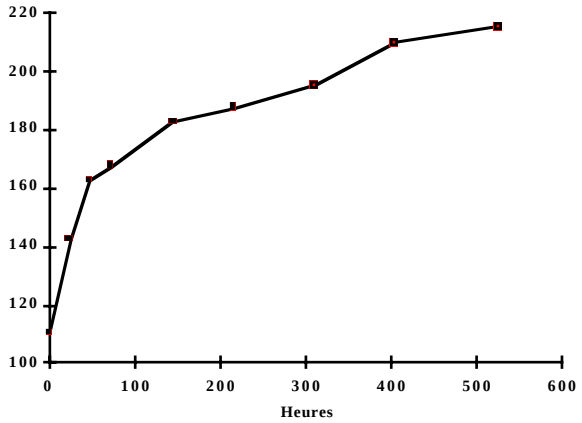

Figure 77: *Poly II tower sagitta variation as function of time. During the first four days one observes a 50 % variation. The creep process don't stop and one has an additional variation of 40 % after one month.*

4.1.3. Interpretation of the measurements and Conclusion.

The tower is a beam of length L and of weight P. To simplify the calculation, the section is supposed to be constant. At a given abscissa x, the section is submitted to a bending momentum M_0 and to a transverse force T_0. One obtains the expression for the sagitta, f, under a load F:

$$\mathbf{f = (P (5/8 + \varepsilon/2) + F (1 + 2\,\varepsilon)) L^3 / 48 R}$$

where $\varepsilon = 12R / SL^2$ is the shear term. ε is small and can be neglected.

The variation of the sagitta under load for the Poly I tower (figure 75) is 4.6 μm per Newton, for a load smaller than 40 Newton's. Above 40 Newton's, it becomes 6 μm per Newton. This may be due to buckling of the upper aluminium skin. From the sagitta formula, one estimates that the rigidity R is equal to 390 Newton m^2. The aluminium skin rigidity without buckling is easy to calculate, one has to take into account the lack of extension of the glued part, one obtains 390 Newton m^2. Consequently, the Shashlik pile rigidity is small and unmeasurable. Using the sagitta measurement of the Poly II prototype, before creep, one finds a rigidity of 580 Newton m^2. It is compatible with the aluminium skin rigidity which is 650 Newton m^2. It is coherent with the Poly I result.

The tower construction using a glued aluminium skin allows production of towers with a very good geometrical shape. The main problem is the lack of stability with the time. The lead and plastic pile up is not a reliable material. A solution consists in putting a 1 MPa pressure over the layers, as in the Protvino prototypes, with an initial packing force of 10 MPa. Such a method may damage the scintillator and the time stability is uncertain. Another solution consists in increasing the rigidity of the glued skin. A good solution would be a carbon composite foil whose low density is also favourable from the point of view of the physics requirements.

4.2. The Shashlik Towers

4.2.1. General geometric considerations

The lateral granularity of the Ecal has to satisfy the physics requirements as well as mechanics and electronics constraints. Taking into account the constraints on the shower position precision, trigger considerations as well as the one related to the mechanical structure itself, the granularity has been defined to be $\Delta\Phi = \Delta\eta = 2\pi/144$. This value leads to a number of 144 towers in Φ and 76 towers in η, for a calorimeter covering the pseudorapidity range up to $|\eta| < 1.66$. The CMS Barrel will require 10944 Shashlik multi-bundle towers divided into 36 sets of 8 towers in Φ and 38 in η.

Each supporting structure defines a super module. The support structure is described in section 4.3.

The tilt angle (3º), necessary to limit the crack effects and the channelling in the WLS fibres, is obtained by rotating each super module, the towers inside being kept projective. A parallel clearance of 4 mm between the super modules is necessary. This value includes the thickness of two 0.5 mm lateral sheets of composite or stainless steel.

The total available space for the Ecal is located between the radius values 1390 mm and 1975 mm inside the CMS hadron calorimeter sitting itself in the 4 Tesla solenoid. This constraint influences a lot the Shashlik tower and support structure design. Figure 78 shows the transversal view of the CMS electromagnetic barrel at $\eta = 0$ and the 18 Super Modules of a half barrel.

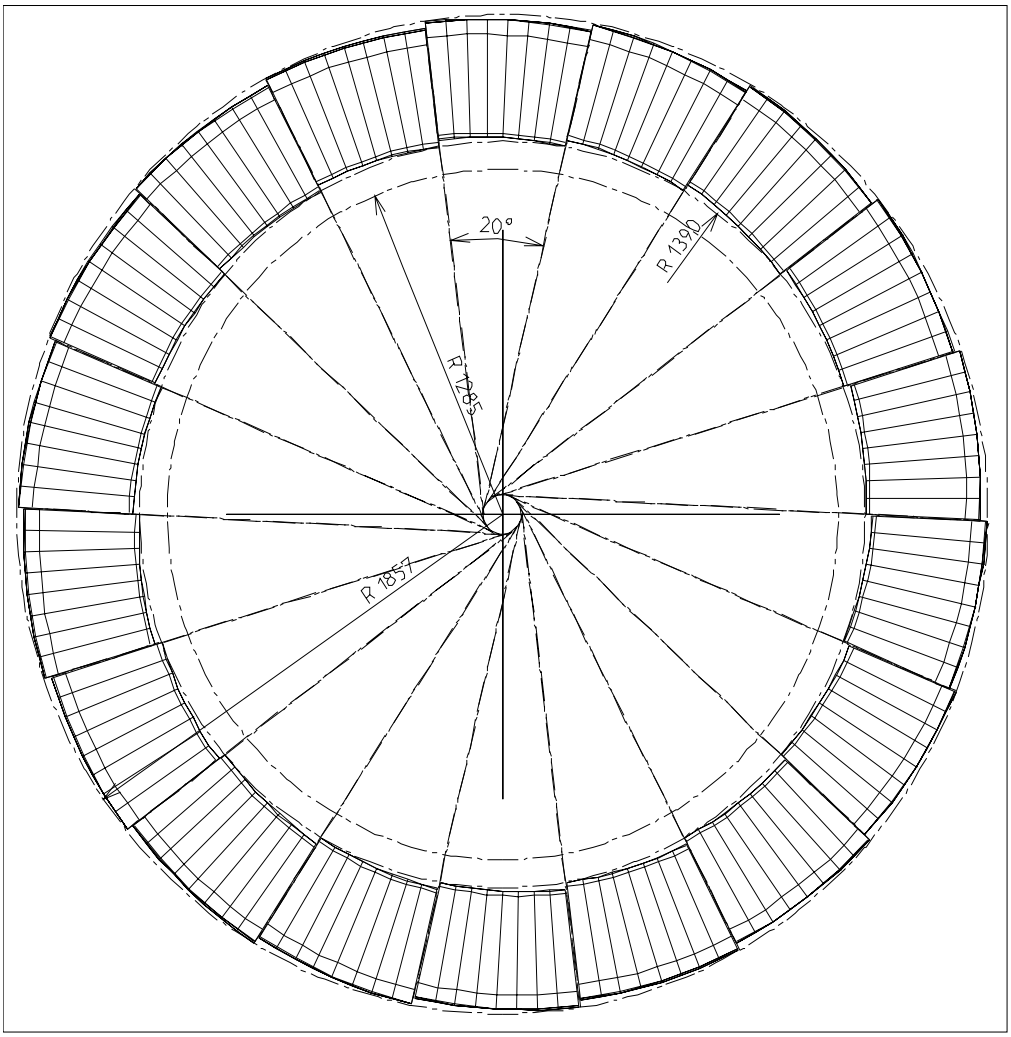

Figure 78: *Transversal view of the CMS electromagnetic barrel at $\eta = 0$ of the 18 Super Modules of a half barrel.*

4.2.2. Shashlik tower components

The required resolution defines the sampling and therefore the thickness of the lead plates (2 mm). The minimal depth required for the shower containment (25 X_0) defines the number of lead plates (70) and radial space (at η=0), the thickness of the scintillator tiles (3 mm). The available space increases with η allowing a smooth increase of the calorimeter depth (30 X_0 and 84 layers).

The lateral dimensions of the pyramidal towers increases as a function of the depth and angles as a function of η. For light collection 100 WLS fibres 1 mm in diameter are foreseen, allowing double or quadruple readout bundle. Consequently all components present a 10 x 10 matrix of holes 1.2 mm in diameter with a 6.4 mm pitch. The size of the standard blanks needs to be 80 x 80 mm^2.

The scintillator tiles are manufactured by injection moulding. This process gives accurate thickness tolerances (better than σ= 6 μm has been achieved for the prototypes), and provides good radiation hardness. Most likely, the holes should be made by drilling.

The mechanical properties of pure lead are very poor, but some alloys may improve them: calcium-tin lead combines physical properties of pure lead and considerably better mechanical properties (strength and creep resistance). The production of this alloy needs carefully controlled chemical composition and metal working parameters. One can obtain directly rolled wound strips 200 x 8 cm^2 with very good thickness tolerances (likely σ=5 μm). Punching the holes and cutting to blank dimensions should be possible in one operation.

Tyvek foils are inserted between the lead and the scintillator in order to insure total reflection. Punching the holes and cutting to blank dimensions is possible in one operation.

4.2.3. Manufacturing process of the Shashlik towers

The stacking operation is done by using the standard blanks (80 x 80 mm^2) of the different basic components of the towers: lead plates, scintillator tiles and tyvek foils. The number of layers, variable with η, has to be respected. The relative positioning of the blanks is essentially ensured by 4 metal rods 1.1 mm in diameter

thread through the peripheral holes of the matrix. Stacking a tower can take as much as two hours of manual work.

The adjustment of the stack length is achieved by compression. This creates a temporary prestress which provides sufficient stiffness during handling operations. A jack compress the stack directly in the Vee in which the blanks are positioned. The clamping at the nominal length is ensured by crimping of the rods.

The assembled stack can be then machined. The aim of this operation is to obtain the final oblique pyramidal shape and to provide a surface texture satisfying the needs optics and gluing. The materials: lead, polystyrene and tyvek are milled simultaneously by means of a special set-up allowing precise positioning and tightness of the stack.

4.2.4. Finishing of the Shashlik towers

In the different Shashlik prototypes, the reflection at the edges was insured by a polished aluminium skin. The carbon epoxy of composite skins ,we intent to use for the tower assembly, will need a special treatment in order to provide a high reflectivity.

Once the tower machining is done, each stack is equipped with a rear and front aluminium mechanical part. These elements gives to the tower its transverse geometric precision and allow the fixation to the support spine as it will be described in section 4.3. These parts would be partly manufactured by injection moulding and finished by milling. The number of rear and front parts (12000) is sufficient to justify an injection moulding process.

The gluing operation of the composite skins completes the mechanical production of the towers. The skins are a major constituent of the Shashlik towers. They join together all the layers of the stack and the extremity parts. They provide a good stiffness and a well defined geometry. Carbon composite epoxy constitutes the best compromise between mechanical and physic's needs. A thickness of 0.4 mm is sufficient to obtain the necessary stiffness. The radiation hard epoxy glue is deposited using a silk-screen printing process. A bounding tool is used, to keep parts to be glued under compression during curing, and to maintain the assembly within the correct geometry. Once the glue is cured, a mechanical control is done to check the quality of the geometry.

The threading of the fibres will have to be done manually. One of the extremities of the fibres is aluminised by sputtering. The other extremities of the fibres are grouped to form a bunch. A support element made of two different parts is necessary to hold the bunch. One part is used to hold the bunch at the right height above the rear face of the Shashlik layers, the other to maintain the fibres grouped. The extremity of the fibres are glued inside it and diamond machining is done to give them a good optical quality.

Individual quality control of each tower follows the manufacturing process. This control includes metrology of the dimensions of the towers and check of the response, using a cobalt source for example.

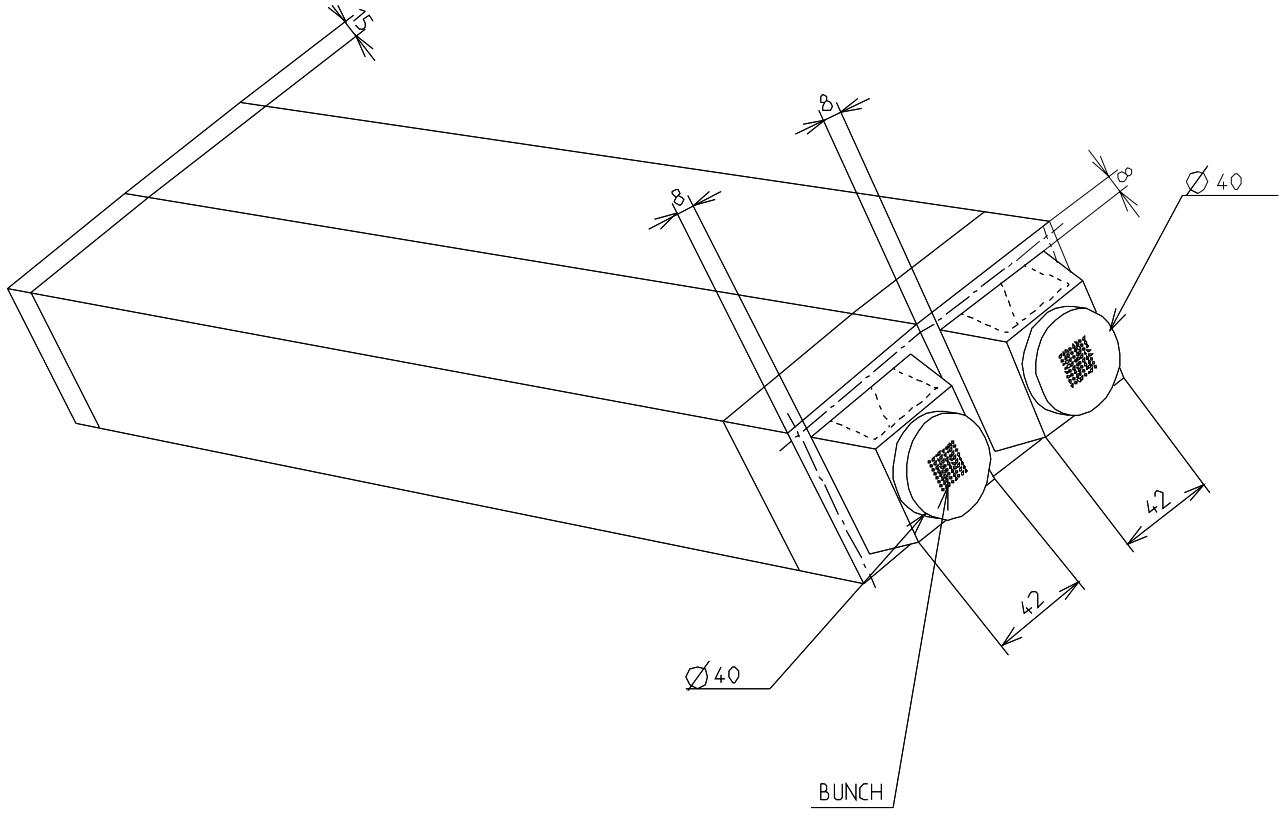

Figure 79: *A couple of Shashlik towers glued together.*

To optimise the mechanical structure of the barrel calorimeter the tower will be glued two by two first as shown on figure 79. Groups of 2 towers glued together for all η will be mounted on the spine described in section 4.3 (figure 83). Four spines defining the super module (figure 84 will define a set of towers as represented on figure 80.

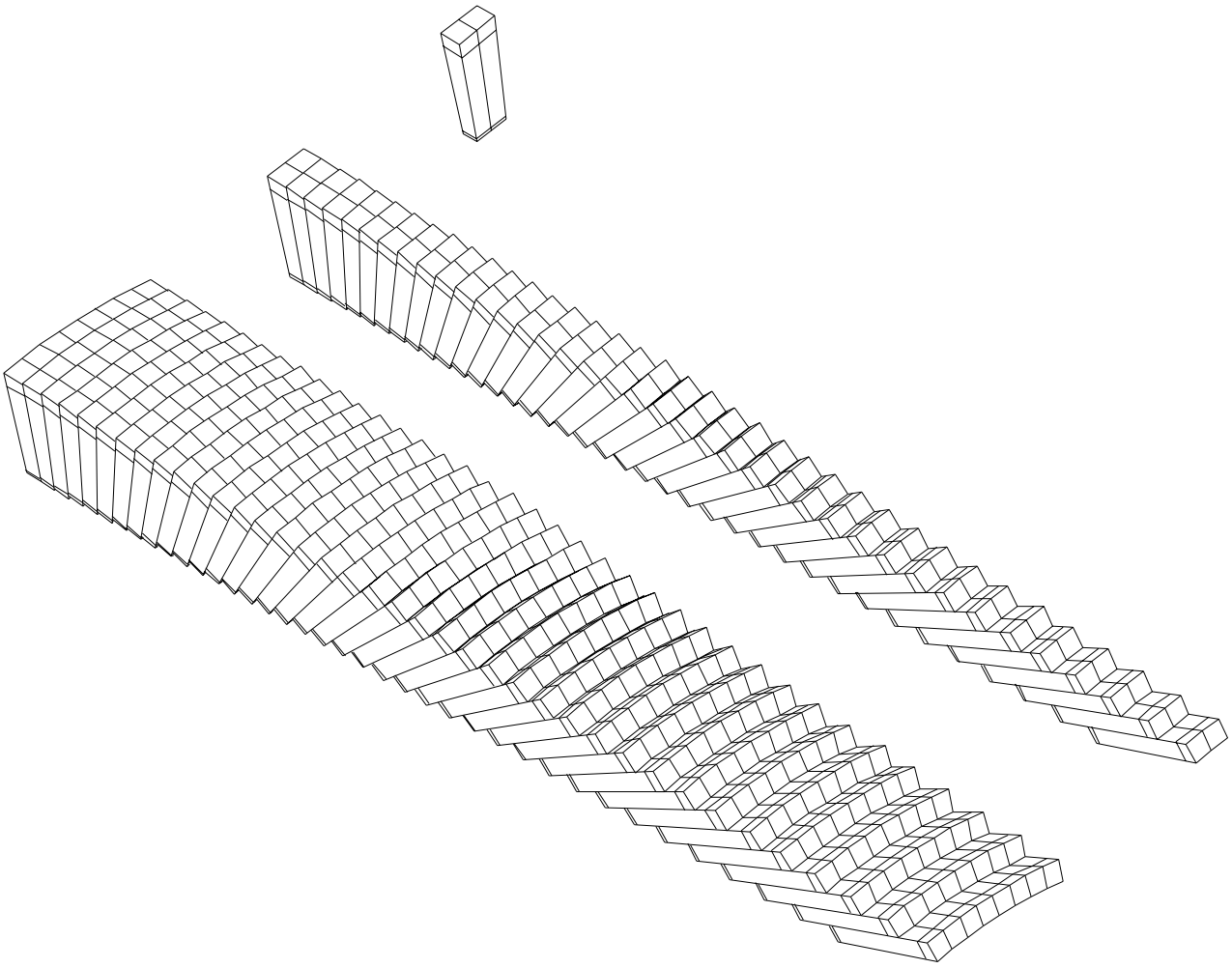

Figure 80: *Sketch of the Shashlik tower assembly.*

4.3. Barrel section support structure for the Shashlik Calorimeter.

4.3.1. Strategic Considerations

A mechanical support structure for the barrel section has been has been designed which achieves a detector modularity with a high degree of symmetry and repetition of individual elements. This leads to a modular size and weight which is compatible with the logistics required for assembly and test in several institutes. It also facilitates the preassembly and calibration of sub sections in test beams at CERN and minimises the size and cost of the special equipment required for installation.

4.3.2. Barrel Section Design

The barrel section of the calorimeter covers the η rapidity interval from zero to 1.66 (22 degrees).

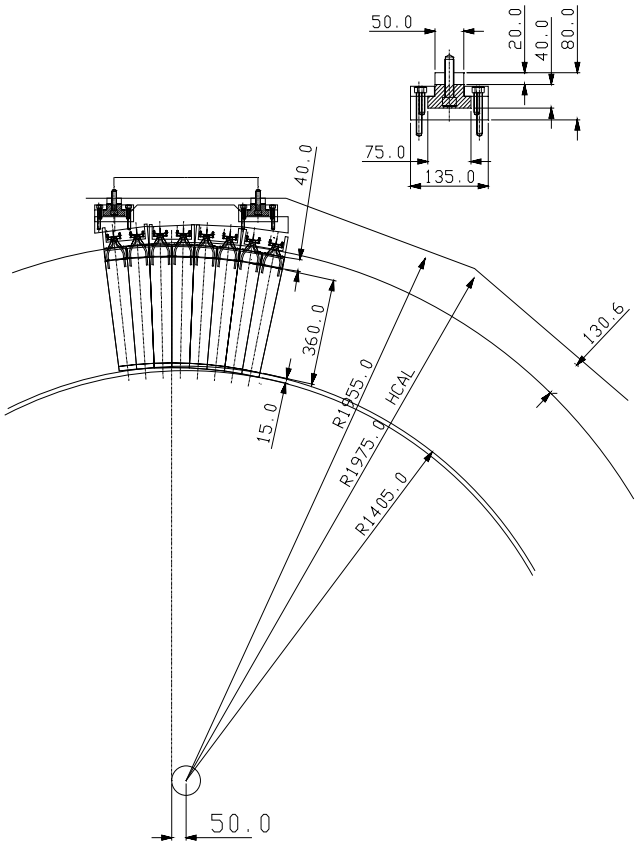

Figure 81: *A Super Module at η=0 in place inside the hadron calorimeter.*

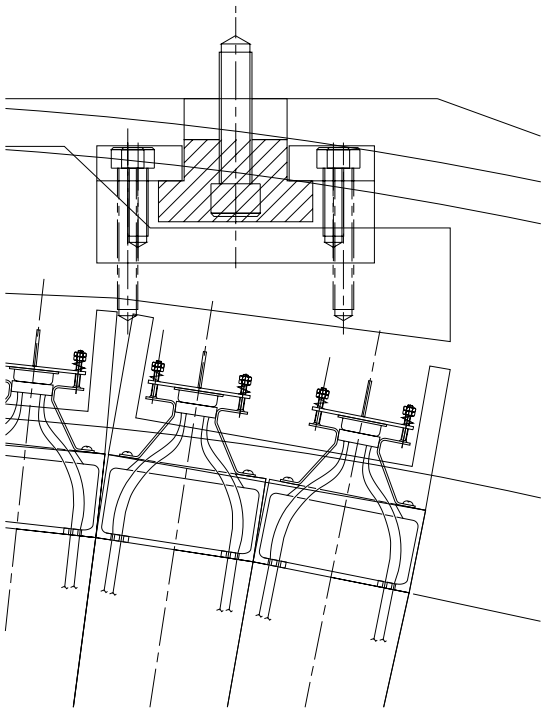

Figure 82: *Detail of the upper part of the towers and their support to the "spine".*

The overall barrel section is subdivided into two identical halves each comprising 38 individual tower elements in eta and 144 individual tower elements in phi (figure 81). Details of the arrangement are shown in figure 82. The granularity has been chosen to optimise both the physics requirements and the need to minimise costs and complexity in producing .

4.3.3. Tower Elements

The Shashlik towers are equipped with rigid back end support plates which are glued to the towers, together with electronic readout and monitoring facilities as shown in figure 79. The back end plate allows each tower to be supported from the rear of the detector. The fixation support provided for the tower elements is designed to fulfil the dual role of both positioning and supporting the weight of the towers. Each tower element can be fully tested on a stand alone basis prior to further assembly.

4.3.4. Spine Sub Assemblies

Pair of individual towers will be held in position and supported by means of a stiff spine support section capable of supporting 38 individual towers arranged in pairs as shown in figure 83.
The pairs of tower elements will be glued together to form a sub module prior to assembly on the spine support and the sub modules glued together sequentially during the fabrication of the spine section. Four spine sections will then be glued together and interconnected by means of a carriage system as shown in figure 84 to form a Supermodule.

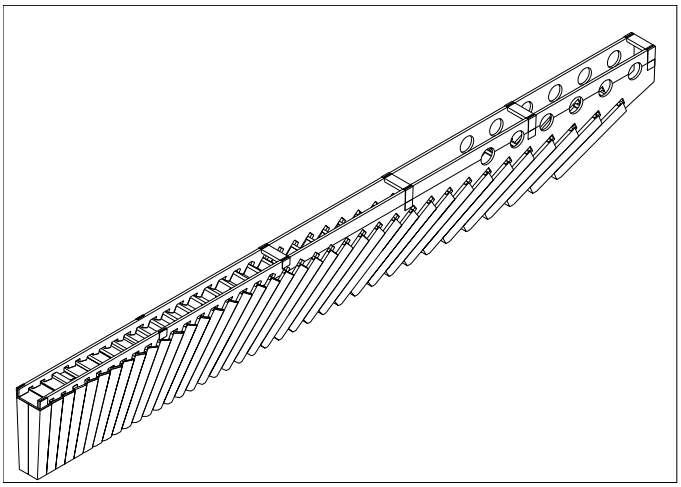

Figure 83: *The spine module suporting 2 x 38 individual towers glued together.*

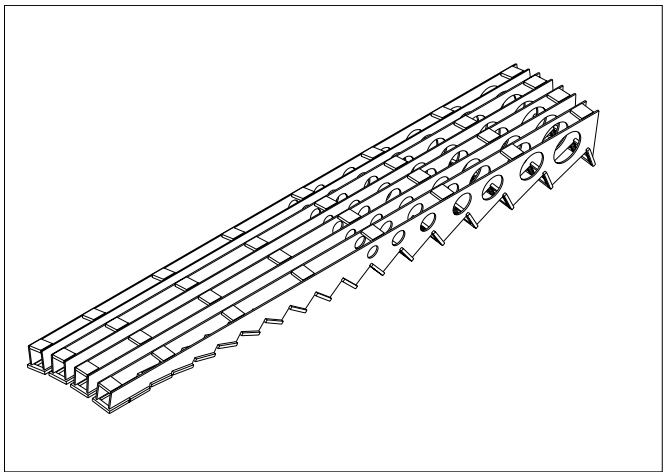

Figure 84: *Assembled 4 spine module defining the super module*

4.3.5. Supermodules

For manufacture and installation purposes each half barrel section will be built up using 18 Supermodules each subtending 20 degrees in phi. The overall planning envisages the fabrication of independent Supermodules fully equipped with electronics, monitor systems and services. The Supermodule sections would be tested at each stage during assembly and commissioning, culminating in a final calibration in the test beam. This approach also allows considerable flexibility during the installation stages of the complete detector. The weight of each Supermodule is estimated to be 3 Tons.

4.3.6. Rail System

The carriage for each Super module (figure 85 will be fitted with the bearing components. There are used to locate the super module to a fixed rail system located on the inner face of the Hadron Calorimeter, as shown in figure 86.

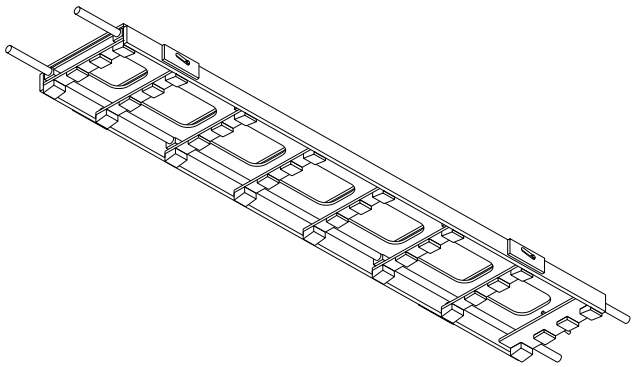

Figure 85: *The carriage for each Super module.*

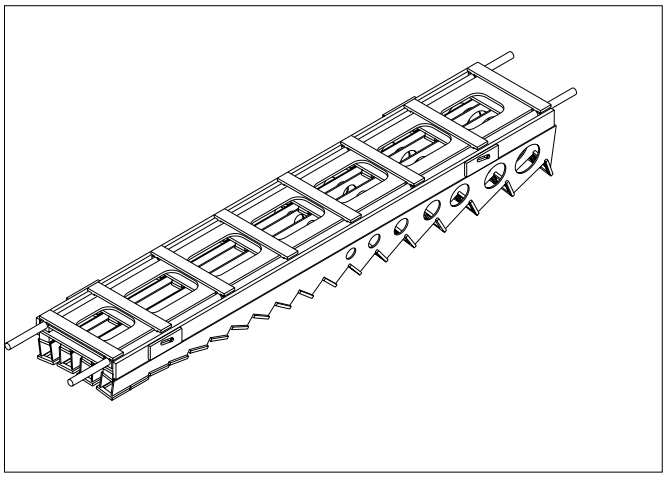

Figure 86: *Assembled super module with the suporting rail system.*

The completed Supermodule assembly can then be installed by insertion from the end of the detector by means of the fixed rail system components fitted to the inner face of the Hadron Calorimeter. The rail system components will be custom designed and fabricated using non magnetic materials. The fixed components will be installed accurately in position using survey and shimming techniques.

4.3.7. Finite Element Analysis

The individual elements of the proposed mechanical support system have been investigated using FEA techniques. The deflections predicted from this analysis were all found to be within acceptable levels.

4.3.8. Summary

The proposed mechanical support arrangements can be implemented using standard manufacturing processes and provide considerable flexibility in meeting the build and installation scenarios foreseen for the CMS experiment.

4.4 EndCap mechanical design.

We present here a possible design for a Shashlik type calorimeter for the CMS Endcap. It is one of the possible designs developed at IHEP (Protvino).

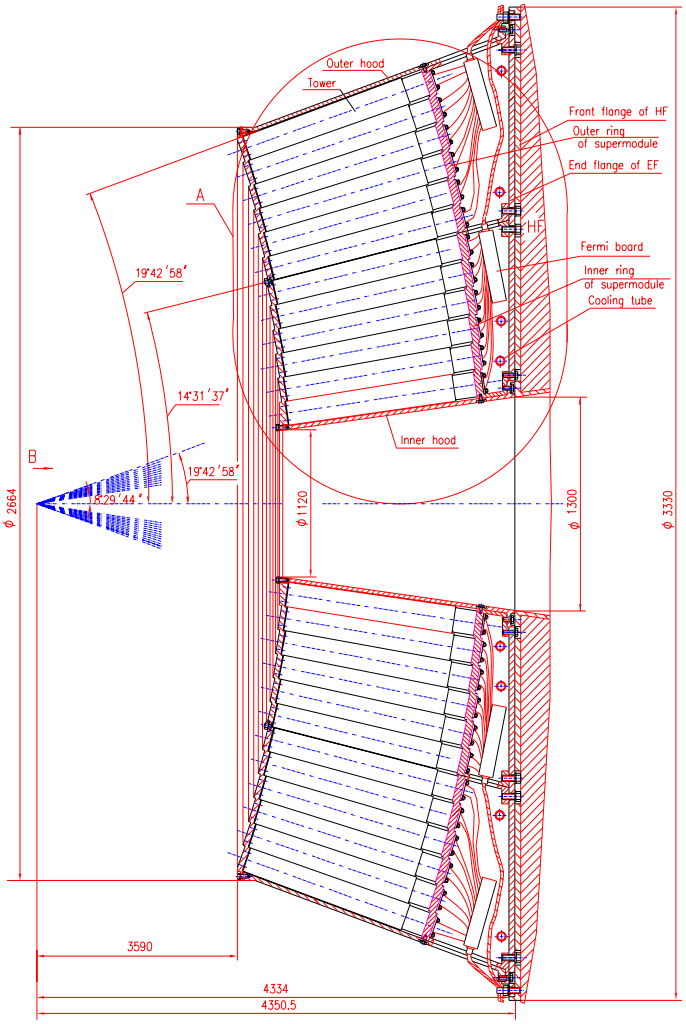

Figure 87: *Shashlik tower EndCap design.*

The main feature of the construction is the possibility of a high precision for the individual alignment of each tower by cantilever fastening. We have chosen a projective tower geometry. The towers are assembled in rings (figures 87). The inner most one (η>2.) has to be easily removable, as it is situated in a region where the radiation level is high and even in the case of a radiation hard scintillator calorimeter a replacement has to be foreseen. Figure 88 shows a details of part of the outer ring. The chosen design minimises the cracks between modules. The amount of material in front of the towers is kept small. The support structure includes a back titanium support flange, an inner and outer cone-shaped frames which are linked by the front flange made of compound material. Windows in the outer cone provide access to the Fermi board and cooling system.

The outer ring Supermodule has a weight of 6 tons and is built out of 864 towers. The inner ring Supermodule is done with 432 towers. Its weight is 4 tons. The tower granularity is the same as for the barrel. We foresee to have multibundle towers built with the same technique as for the Barrel.

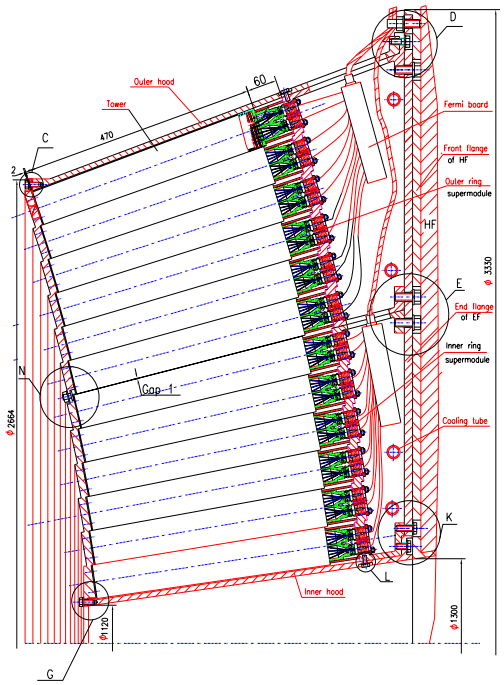

Figure 88: *Supermodule of the Shashlik tower EndCap design*

4.5. The Preshower Detector Mechanical design

4.5.1. Basic design

The design of the preshower presented below has been optimised for the case of the Shashlik calorimeter. The preshower contains 2 planes of silicon strip detectors inserted in a lead converter. There are 2 radiation lengths of material before the first Silicon plane, followed by another radiation length between the first and the second plane. The strips of the 2 planes are orthogonal. The first plane measures the ϕ coordinate, while the second plane measures the z coordinate along the beam axis. An important aspect of the design is the compactness of the detector, particularly in the barrel part. In this region, the magnetic field, which is almost perpendicular to the particles direction, produces an opening of the shower and bends the low energy electrons created in the cascade. It has been shown by Monte Carlo simulations that the key parameter is the distance between the Silicon plane and the preceding lead converter, which must be kept to a minimum. Also important, but to a smaller extent, is the overall distance of the preshower to the front face of the calorimeter.

The sensitive planes are built from 6x6 cm^2 wafers of npn type silicon, which contain 32 strips each. The pitch of the strips is 2 mm. In the barrel, where the strip occupancy is low, the strips of 2 adjacent wafers are connected together, to build 120 mm long strips. In each layer, the wafers overlap in one view to reduce the dead space due to the guard rings. The silicon wafers are glued on a ceramic, which is fixed to an aluminium support: this structure should allow an efficient cooling of the silicon. Further studies are necessary to choose the optimal thickness of the silicon: our prototypes are actually 400 μ thick, but a 300 μ thickness may be preferable in view of the radiation properties.

4.5.2. Barrel Mechanics

The Barrel preshower detector is an independent cylindrical instrument which is divided into 36 preshower-super modules.

These modules are connected to the front-end of the Shashlik-Super module.
The preshower super-module is self-supporting but needs a support frame for transport and manipulation. When mounted it will get its position and extra stiffness from the Shashlik Super module. All the services, cables, etc. are arranged per super module.
The main parameter of the preshower super module are given in table 6.

Preshower	Super module
Inner radius	1330 mm
Outer radius	1390 mm
Length	2900 mm
weight	<300 kg
Si-wafers	2x400=800 pC.

Table 6: *Main parameter of the preshower super module*

A cross-section of the Preshower detector is shown in figures 89 and 90 for η=0 and η=1.66.

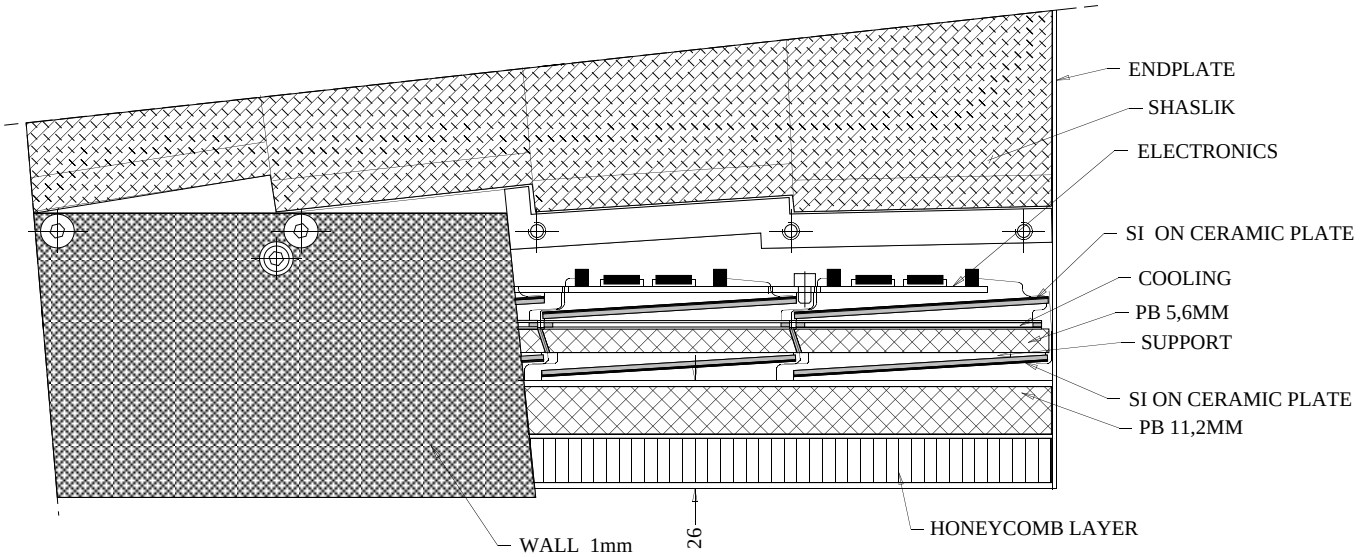

Figure 89: *Preshower super module section at η =0*

It consists out of the following elements:

The honeycomb and the first layer of lead

By gluing a honeycomb and the first layer of Pb together with 2 skin-plates we get a sandwich structure which will work as the support for the preshower Super module.
The thickness of this support-structure is 26 mm with a length of 2900 mm.
The thickness of the Pb will decrease from 11.2 mm to 4 mm continuously along the beam axis, the thickness of

the honeycomb(very light material) will increase to compensate the loss in thickness.
The outside surface of the support is like two inclined planes to ease the mounting of the different preshower elements.

The Si layers, the second layer of Pb and the Si cooling

The first and second Si layers are mechanically identical. They are glued via a ceramic-plate on an extruded Al profile. The shape of the profile allows an overlap in z.
On each profile there are 4 Si wafers (figure 91) 2x8 profiles are glued on both sides of a structure consisting of the second lead plate and a cooling-layer. This assembly represents a "panel" of dimensions of 24 cm x 48 cm. In each super module we have 2 (in ϕ) x 6(in z) panels. Since the thickness of the second layer of lead varies from 5.6 to 2 mm along the beam-axis, the thickness of the various panels will also vary.

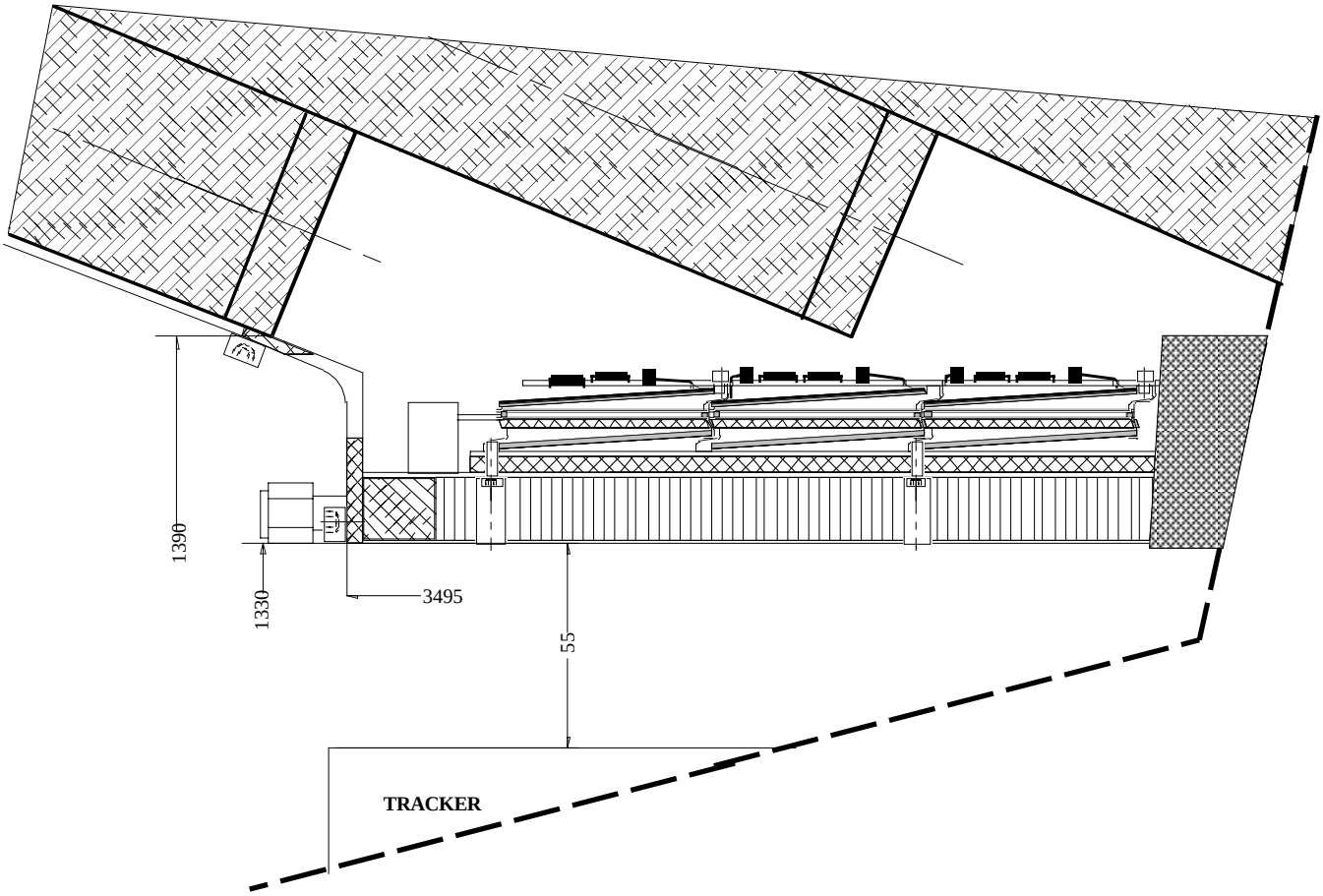

Figure 90: *Preshower super module section at η=1.66*

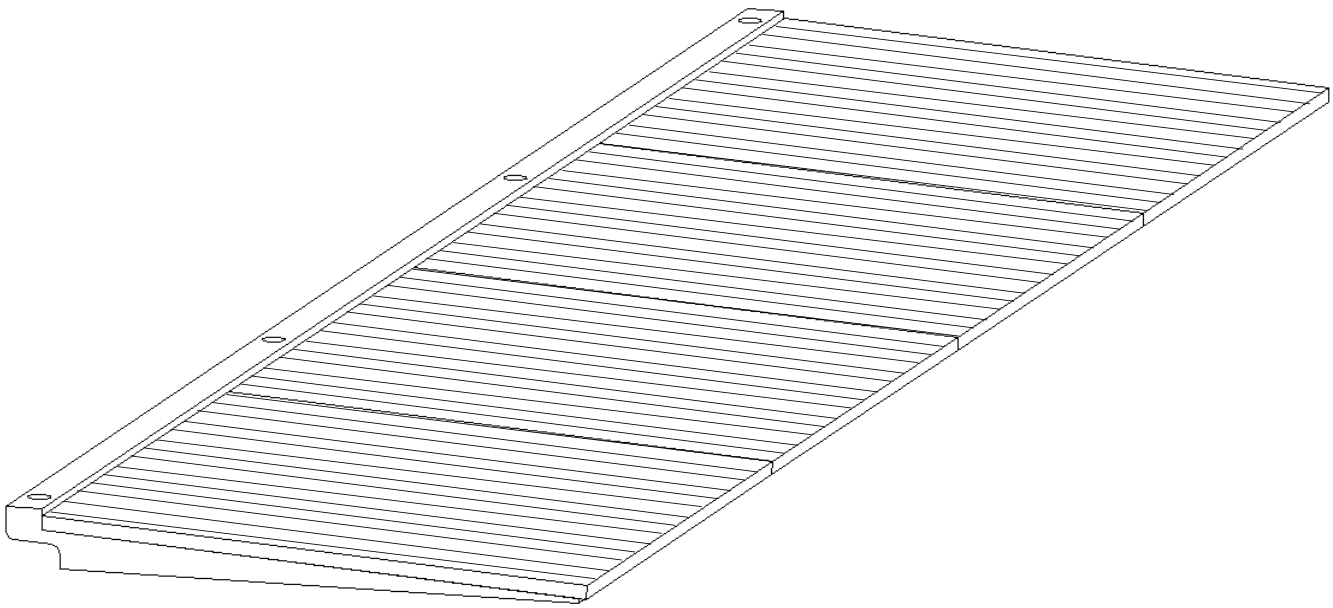

Figure 91: *Preshower silicon wafer profile out of 4 Si-wafers*

The electronics is located on PCB's placed directly above the second layer of Si detectors. The strips are connected to the electronics via a flat cable. For the first layer of Si, these cables have to pass through the second layer of lead. For this purpose there are 1.5 mm wide slots in this lead plate. The PCB's can be connected to the structure with screws.
The connection between the Shashlik and Preshower super modules is done by three different elements: the two side walls of the calorimeter super module (see figure 89) with a thickness of 1 mm, the two endplates (see figure 89 and 90) and by a few bolts accessible by holes in the walls.

4.5.3. Number of electronics channels

In the barrel, each of the 36 super modules contains 400 6x6 cm^2 wafers *per layer*. Each wafer has 32 strips. We connect 2 wafers together, to build 12 cm long strips: the number of electronics channels is therefore 6400 per Super module and per layer. Since we have 2 layers measuring orthogonal coordinate we obtain a total of 460800 channels. In the end caps, we will stick to 6 cm long strips: the total number of electronics channels for the 2 end caps, assuming 2 layers of Silicon per end cap, is approx. 160000.

4.5.4 Radiation tolerance of Silicon detectors

Neutron fluences and doses have been evaluated recently at the preshower level for the case of the $PbWO_4$ calorimeter. These evaluations show that it is important to shield the preshower with neutron moderators situated between the preshower and the ECAL. The thickness of the polyethylene moderator varies from 2 cm in the barrel to 4 cm in the forward preshower, at η=2.6. In this case one computes a total fluence of 2 10^{13} hadrons/cm^2 in the barrel, and up to 10^{14} hadrons/cm^2 in the forward preshower, after 10 years of irradiation.
At room temperature, one would expect[3.9] a large leakage current after irradiation : about 15 $\mu A/cm^2$ in the barrel and 75 $\mu A/cm^2$ in the forward region, for 300 μm thick Silicon. It would also be necessary to increase the bias voltage above the initial depletion voltage by about 50 V in the barrel and 240V in the forward. These numbers are very close to the limit in the barrel and unacceptably large in the end-caps. We must therefore keep the Silicon at a lower temperature. The following table summarises the expected parameters regarding radiation damages to the Silicon detector for 2 different detector thicknesses.

	Barrel	**Forward** (worst case η=2.6)
Temperature	10 °C	5°C
Leakage current		
Si 300 μ	5 $\mu A/cm^2$	20 $\mu A/cm^2$
Si 400 μ	7 $\mu A/cm^2$	25 $\mu A/cm^2$
Increase of Bias Voltage		
Si 300 μ	30 V	+70 V
Si 400 μ	50 V	+130 V
Power dissipation/channel in Silicon		
area	2.4 cm^2	1.2 cm^2
Si 300 μ	0.5 mW	3.5 mW
Si 400 μ	1.1 mW	8 mW

Table 7: *Expected parameters regarding radiation damages to the Silicon detector for 2 different detector thicknesses.*

It should be noted that these figures are based on high flux irradiation measurements, extrapolated for the long term evolution. Further irradiation's studies are going on in order to optimise the long term operation of Silicon detectors.

5. Future programme

The next year will bring the R&D to a final stage mainly by optimising the technologies of the readout system for both the Shashlik and the preshower detector.

Shashlik calorimeter:

- ***Improvement in Quality and Production***

We still expect to improve the light yield and uniformity of response of the towers under construction (4-6 towers). Multibundle towers with 4 independent readouts will be build using the construction process described in section 4.2.

- ***Photodetectors and Electronics Chain***

Photodetectors

In addition to the work on PIN photodiode readout, the design of both APDs and vacuum photodetectors have to be optimised in collaboration with the manufacturers. Radiation damage and ageing tests of both types of photodetectors have to be performed. For the APDs various schemes for temperature and voltage stabilisation will be tested. The field dependence of the gain of vacuum photodetectors will be measured at various orientations in fields up to 4 T.

Front End Electronics

During 1995 prototypes of preamplifiers, shapers and compressors as well as the FERMI analog ASICs, in the form of a three-channel VME board, will be evaluated in beam tests together with the photodetectors.

- ***Beam Tests***

In 1995 detailed measurements of the energy resolution and angular resolution on multibundle towers will be carried out, with and without a preshower. This will be done with the large 6 x 6 matrix described in this report by replacing 9 of the central towers by 4 multibundle ones. It is clear that the dimensions of the new towers will be chosen to allow this exchange. The tests will employ different types of APDs and PINs photodiodes. Combined tests with the HCAL are also envisaged.

- ***Radiation hardness Tests***

In 1995 we will continue the radiation hardness studies on Shashlik towers. In particular we will receive new towers built with radiation hard scintillator. The process will be to measure first the energy resolution response and uniformity of a tower, irradiate and then remeasure the energy resolution response and uniformity.

Preshower:

Preshower Electronics

In 1995, we will first test the various chips which have been submitted in 1994 (see section 3):
• the radiation hard versions of the Icon amplifier in SOI and DMILL technology , to be received during Spring 1995. A radiation hard technology will be selected from the results of these tests.
• the MIETEC version of the Analogue Memory (DYN1), which we just got at the end of 1994.
• the rad hard Thomson CRIAD ADC.

Following these tests, we intend to submit during the fall new versions of the chips, with increased functionality. We will continue our investigations on the digital processing and we will complete the computer modelling of the whole electronics chain.

Silicon detectors

In parallel, more work has to be devoted to the Silicon detectors themselves and their radiation hardness.
We would like to study Silicon wafers from various suppliers and investigate (for example) lower receptivity Silicons.

6. Conclusions

New techniques have been developed to read out the light from lead/scintillator sampling calorimeters. These techniques involve the use of wavelength shifting optical fibres. The use of optical fibres enables fine lateral segmentation to be achieved with a minimum of dead space. In addition, it was expected and now confirmed that such calorimeter can be built at a relatively low cost. A good optimised mechanical design was studied for the CMS electromagnetic calorimeter. Several new projective prototypes have been built and tested in electron beams at CERN. The light yields are in excess of 20 photons per MeV. The uniformity of the response has also been investigated on an area of 20x15 cm^2. A mean dispersion of less than ±1% has been achieved. Prototype towers were also studied in magnetic field (up to 3 Tesla). An increase of the calorimeter response of ≈10% has been observed. No degradation of the performance of the calorimeter has been found. The energy resolution measured on projective towers (42x42mm^2 at front face) from our last 6x6 matrix prototype is:

$$\frac{\sigma}{E} = \frac{.08}{\sqrt{E}} \oplus \frac{.3}{E} \oplus 0.005 \qquad \left(E \quad \text{in GeV}\right)$$

Several towers were also measured in beam after irradiation with 500 MeV electrons produced at LiL. An irradiation of 1 Mrad (10 years of LHC at nominal luminosity in the CMS barrel) produce a loss of light of about 10%. The loss of energy resolution has been found to be small.

We have also developed and studied multi-bundle Shashlik towers. This technique allows to build larger size towers (6x6cm^2 are foreseen for the CMS barrel) readout with 2 to 4 WLS bundle of fibres giving: redundancy in the readout, improvement in the shower position resolution, angular resolution..., without losing any precision in the energy resolution.

Another goal of RD36 is to study the preshower detector which will be placed in front of the calorimeter. The preshower consists of two layers of lead radiators followed by Silicon strip detectors. The aim of the preshower is to measure accurately the shower position and to provide some separation between single photons and π^0. Together with the position measurement in the calorimeter, the preshower allows a measurement of the shower direction. In 1994, tests were made with a 3 X_0 thick preshower containing 2 planes of Silicon, covering a transverse area of 12x12cm^2 A good position resolution (≈300 μm at 80 GeV) has been obtained. Using the shower barycenter position deduced from energy deposited in the calorimeter and the position measured in the preshower we achieved an angular resolution of:

$$\sigma_\theta(\text{mrad}) = \approx \frac{60}{\sqrt{E}} \qquad \text{(E in GeV)}$$

It was shown that the energy loss in the lead radiators can be measured in the Silicon and corrected for, so that the energy resolution of the Shashlik calorimeter is only slightly degraded when the preshower detector is added, even when the detector is put in a high magnetic field.

The measured performance of a Shashlik+Preshower detector satisfies the requirements demanded of a sampling calorimeter at the LHC.

References

1.1 • C. Seez *et al*, Proc. Large Hadron Collider Workshop, Aachen, 1990, eds. G. Jarlskog and D. Rein, CERN 90–10, vol. III, 474

1.2 • CMS Letter of Intent, CERN/LHCC 92-3, LHCC/I1, October 1992
• CMS Status Report and Milestones, CMS Collaboration, CERN/LHCC 93-48 (1993).
• CMS Status Report and Milestones, CMS Collaboration, CERN/LHCC 94-20 (1994).
• Technical Proposal, CMS Collaboration, CERN/LHCC 94-38 (1994).

1.3 • A combined Shashlik + Preshower detector for LHC. CERN-DRDC Proposal P50. CERN/DRDC 93-28 (1993).

1.4 • Influence of dead materials and cracks in the performence of the CMS electromagnetic calorimeter. CMS TN /94-176

2.1 • E. Beuville et al., Nucl.Instr.and Meth., A288 (1990) 157.
• E. Beuville at all. Nuclear Physics B. (Proc. Suppl.) 23A(1991) 198

2.2 • R. Tanaka IV International Conference on Calorimetry in High Energy Physics. La Biola d'Elba, Italy(1993).

2.3 • Shashlik calorimeter. Response to high energy electrons. NIM A 344(1994) 57-63

2.4 • Shashlik calorimeter. Beam test results. NIM A 348(1994) 74-86
• J. Badier et al., "Shashlik calorimeter beam test results", CMS TN/93-66, X-LPNHE/93-04 (1993).
• J. Badier et al., "New Test Beam Results of Shashlik and Preshower Prototypes", CMS TN/94-152 (1994), INR-984/94, X-LPNHE/94-01.
• First beam test results from the Spakebab electromagnetic calorimeter. CMS-TN/94-245
• Study of Light Collection as Function of Shashlik Tile Size. CMS-TN/94-240
• Stresses calculations for a glued Shashlik calorimeter. CMS-TN/94-196

2.5 • Multi-Bundle Shashlik calorimeter prototypes. Beam-test results. CMS-TN/94-197. To be pub. in NIM

2.6 • New test beam results of Shashlik and preshower prototypes. CMS-TN/94-152

2.7 • Shashlik calorimeter for CMS. CMS-TN/93-127. IV International Conference on Calorimetry in High Energy Physics. La Biola d'Elba, Italy(1993).

2.8 •J.Badier et al., "A Lead/Scintillating Fiber Electromagnetic Calorimeter for CMS", CMS TN/92-13 (1992).

2.9 • Shashlik energy resolution with and without Magnetic Field. CMS TN /95-002

2.10 • Study of the Shashlik uniformity response. CMS TN/94-311
• Design and performence of a Shashlik calorimeter for CMS. CMS TN/94-305

2.11 • J.Mainusch et al., Nucl.Instr.and Meth., A312 (1992) 451.

2.12 • D.Blomker et al., IEEE Trans.Nucl.Sci.NS-37(2) (1990) 220.

2.13 • E.Guschin,Yu.Musienko,I.Semenjuk. INR-1005/94
preprint (Institute for Nuclear Researches,Moscow,1994).

2.14 • E.Guschin et al., CERN--CMS TN/93-108 (1993).
• A.Karar, CERN--CMS TN/93-96(1993) and Proceedings of the IV International Conference on Calorimetery in High Energy Physics (La Biodala, Isola d'Elba,Italy,September,19-25,1993).

2.15 • E.Guschin,Yu.Musienko,I.Semenjuk. INR-1005/94
preprint (Institute for Nuclear Researches,Moscow,1994).

2.16 • First beam test results from the Spakebab electromagnetic calorimetr. CMS TN /94-245

2.17 • Neutron and photon fluxes and sheildingalternatives for the CMS detector at LHC, CMS TN/94-241, 1994

2.18 • New results on plastic scintillators radiation damage, CMS TN94-220, 1994
• Radiation hardness of WLS-fibres, CMS TN/94-221, 1994

2.19 • Gamma-irradiation tests of Shashlik electromagnetic calorimeterinjection moulding type scintillators, CMS TN/94-225, 1994

2.20 • Britvich et al, *Nucl.Instrum. and Meth.***A326** (1993) 483

2.21 • F. Markly etal, *Radiat.Phys. and Chem.* **41** (1993) 135
• J.P. Harmon et al, *Radiat.Phys. and Chem.* **41** (1993) 153

2.22 • Radiation hardness of Shashlik calorimeter, CMS TN/93-97, 1993

2.23 • G.Anzivino et al, *Nucl.Instrum. and Meth.* A346 (1994) 153

2.24 • Study of the light collection in Shashlik electromagnetic calorimeter radiation damaged perforated scintillators, CMS TN/94-224, 1994

2.25 • LiL beam test Facility and Radiation Hardness tests. CMS TN /94-262

2.26 • Gamma irradiation tests of a Shashlik Ecal injection molding type scintillators. CMS TN /94-225

2.27 • Radiation hardness of WLS fibres. CMS TN/94-221

2.28 • New results on plastic scintillators radiation damage. CMS TN /94-220

3.1 • CERN / DRDC 94-31, RD9 status report 3 / 8 / 94
• CERN / DRDC 93-17, RD9 status report 3 / 3 / 93
• CERN / DRDC 92-15, RD9 status report 10 / 3 / 92
• CERN / DRDC 90-79, RD9 proposal 11 / 12 / 90

3.2 • CERN / DRDC 93-45, RD29 status report 18 / 10 / 93
• CERN / DRDC 92-31, RD29 P42 proposal 14 / 5 / 92

3.3 • CERN / DRDC 94-34, RD2 status report 12 / 8 / 94
• CERN / DRDC 93-18, RD2 status report 18 / 3 / 93
• CERN / DRDC 92-4, RD2 status report 4 / 1 / 92
• CERN / DRDC 90-27, RD2 proposal 1990

3.4 • A Low votage, low power 2MHz CMOS comparator 12 bits ADC. P.Anghinolfi et. al, ISCAS proceedings 1994, London May 1994

3.5 • CERN / DRDC 94-38, RD23 status report 6 / 10 / 94
• CERN / DRDC 93-35, RD23 status report

3.6 • Anghinolfi et. al, ICON, a current mode preamplifier in CMOS technology for use with high rate particle detectors. 1991. Proceedings IEEE Trans. Nucl. Sci. 39 (1992) 626-633 (Shelf no: CERN ECP 91-25)

3.7 • Anghinolfi et.al,DYN1: a 66MHz front-end analog memory chip with first-level trigger capture for use in future high-luminosity particle physics experiments. 1993. Proceedings / Ed by Navarria, P G Pelfer Nucl. Instrum. Methods Phys. Res., 344 (1994) 173-179 (Shelf no: CERN ECP 93-16).

3.8 • Low power 11 bit 5 Mhz Piecewise Linear A / D converter. P. Deval et, al.

3.9 • Study of the characteristics of silicon detectors irradiated with 24 GeV / c protons between -20C and +20C, F. Lemeilleur et,al. 6th Pisa meeting on advanced detectors, La biodola, Italy, 22-28 May 1994
• Patrick Roy, M.Sc Thesis Uni of Montreal,Avril 1994.Etude de la reponse en courant des detecteurs silicium operes en environnement de tres hautes radiations.

3.9 • Study of the characteristics of silicon detectors irradiated with 24 GeV / c protons between -20C and +20C, F. Lemeilleur et,al. 6th Pisa meeting on advanced detectors, La biodola, Italy, 22-28 May 1994
• Patrick Roy, M.Sc Thesis Uni of Montreal,Avril 1994.Etude de la reponse en courant des detecteurs silicium operes en environnement de tres hautes radiations.